

International
Progress Report

IPR-06-36

Äspö Hard Rock Laboratory

Prototype Repository

Acoustic emission and ultrasonic
monitoring results from deposition
hole DA3545G01 in the Prototype
Repository between April 2006
and September 2006

J.R. Haycox
W.S. Pettitt
Applied Seismology Consultants

December 2006

Svensk Kärnbränslehantering AB

Swedish Nuclear Fuel
and Waste Management Co
Box 5864
SE-102 40 Stockholm Sweden
Tel 08-459 84 00
+46 8 459 84 00
Fax 08-661 57 19
+46 8 661 57 19



**Äspö Hard Rock
Laboratory**

Report no.
IPR-06-36

Author
**J.R. Haycox
W.S. Pettitt**

Checked by
**Lars-Erik Johannesson
R.P. Young**

Approved
Anders Sjöland

No.
F63K
Date
December 2006

Date
January 2007

Date
2007-01-25

Äspö Hard Rock Laboratory

Prototype Repository

Acoustic emission and ultrasonic monitoring results from deposition hole DA3545G01 in the Prototype Repository between April 2006 and September 2006

J.R. Haycox
W.S. Pettitt
Applied Seismology Consultants

December 2006

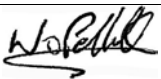
Keywords: Field test, Prototype Repository, Acoustic emission, Ultrasonic monitoring, P-wave velocity, S-wave velocity, Rock fractures, Rock properties

This report concerns a study which was conducted for SKB. The conclusions and viewpoints presented in the report are those of the author(s) and do not necessarily coincide with those of the client.

Report DLV-06-14

**To
SKB**

APPLIED SEISMOLOGY CONSULTANTS

Last Edited	16 January 2007
File name	SKB Proto_Apr06-Sep06_22122006.doc
Last Printed	17 January 2007
Signature	

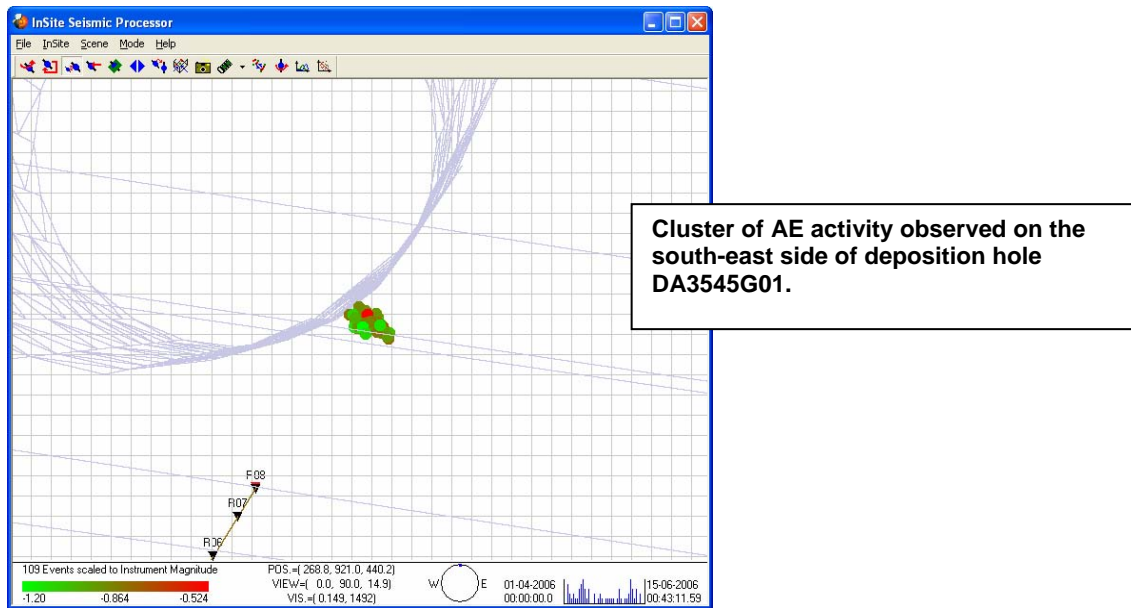
Executive summary

The Prototype Repository Experiment at SKB's Hard Rock Laboratory (HRL), Sweden has been designed to simulate a disposal tunnel in a real deep repository for disposal of high-level radioactive waste. The experiment consists of a 90m long, 5m diameter sub-horizontal tunnel excavated in a dioritic granite. The Prototype Repository design incorporates six full-scale canister deposition holes, excavated vertically into the floor of the tunnel

This report describes results from acoustic emission (AE) and ultrasonic monitoring around canister deposition hole (DA3545G01) in the Prototype Repository. The monitoring aims to examine changes in the rock mass caused by an experimental repository environment, in particular due to thermal stresses induced from canister heating and pore pressures induced from tunnel sealing. This report relates to the period between 1st April 2006 and 30th September 2006, and is the third of an ongoing 6-monthly processing and interpretation of the results for the experiment. Ultrasonic monitoring has been conducted at the Prototype Repository since September 1999. During excavation, monitoring of both deposition holes in section 2 was undertaken to delineate zones of stress related fracturing and quantitatively measure fracturing in the damaged zone. A permanent ultrasonic array was installed in the rock mass in June 2002 around deposition hole DA3545G01.

Ultrasonic surveys are used to 'actively' examine the rock. Velocity changes are measured between transmitter-receiver pairs using a cross-correlation technique that allows a velocity resolution of $\pm 2\text{m.s}^{-1}$. Amplitude and velocity changes on the ray paths can then be interpreted in terms of changes in the material properties of the rock. Calculations using the velocities can determine the changes in dynamic moduli, Young's modulus and Poisson's ratio, to give direct indications of the properties of the rock through which the raypaths travel. Crack density and saturation can also be calculated to determine changes in crack properties in the damaged and disturbed zones. Very little change in P- or S-wave velocity is measured during this monitoring period. The overall trend is for the average P- and S-wave velocity measured between all transmitter-receiver pairs to increase such that velocity is 1.25m.s^{-1} faster for P-wave and 0.70m.s^{-1} faster for S-wave, than at the start. Some larger velocity changes are observed through localised volumes on individual ray paths. P- and S-wave amplitudes decrease initially in the first month then gradually increase over the remaining time. The changes in amplitude are less than were recorded during the previous six month reporting period.

Changes in Young's Modulus, Poisson's Ratio, Crack Density and Saturation Parameters have been calculated from the average measured velocities for different raypath categories. Saturation is observed to increase to a greater extent on raypaths passing through the region of low compressive or tensile stress, and through a possible region of tensile fracturing. This increase may be a result of the slow increase in pressure that could be pressurising fluid into the cracks from the deposition hole. Overall during this six month period, the velocity and amplitude results have shown that the rock mass around the deposition hole has not altered significantly. Gradual increases in temperature and pressure have led to a slow stiffening of the rock, alongside a similarly slow reduction in crack density. During a relatively stable period of environmental characteristics, no dramatic changes in the rock mass have been measured.



During the six-month period, 122 acoustic emissions have been located with high confidence from 151 triggered events. Peaks in activity, in which 4 triggers are recorded on one day, are observed twice on the 18th April and 3rd June. The cumulative plot shows that the rate of triggers remains reasonably constant. On average, 0.98 triggers were recorded per day. An average of 0.80 events is located per day, an increase from the previous 18 months. Study of the spatial distribution of AEs shows 109 of the 122 located events locate in a very tight cluster at a depth of between 455.1 and 455.2m on the south-east of deposition hole DA3545G01. The cluster locates in a region of low-compressive or tensile stresses. The events are close enough together to be considered occurring on the same feature and occur over the whole reporting period with no significant peaks in activity. AEs may be occurring at this position due to the presence of a pre-existing microcrack, generated during excavation. Alternatively, the events may result from movement of an instrument positioned on the deposition hole wall.

For the past year, a greater proportion of events have been locating in the low-compressive regions in the NW and SE quadrants. During excavation and initial heating, the majority of the events located in the NE and SW quadrants. These regions are subject to increased compressive stresses. Smaller clusters were observed in the orthogonal regions of low-compressive or tensile stress. It is important to note that events located during this reporting period are consistent with previous results, i.e. no events are positioned in regions where activity has not been observed in the past. The events can therefore be interpreted as a continuation of activity in the damage zone, and are created either by movement on pre-existing microcracks, or as a result of extension or formation of new microcracks in the existing damaged region. The numbers of events are relatively low and therefore indicate the rock mass around the deposition holes has remained stable during this six-month period.

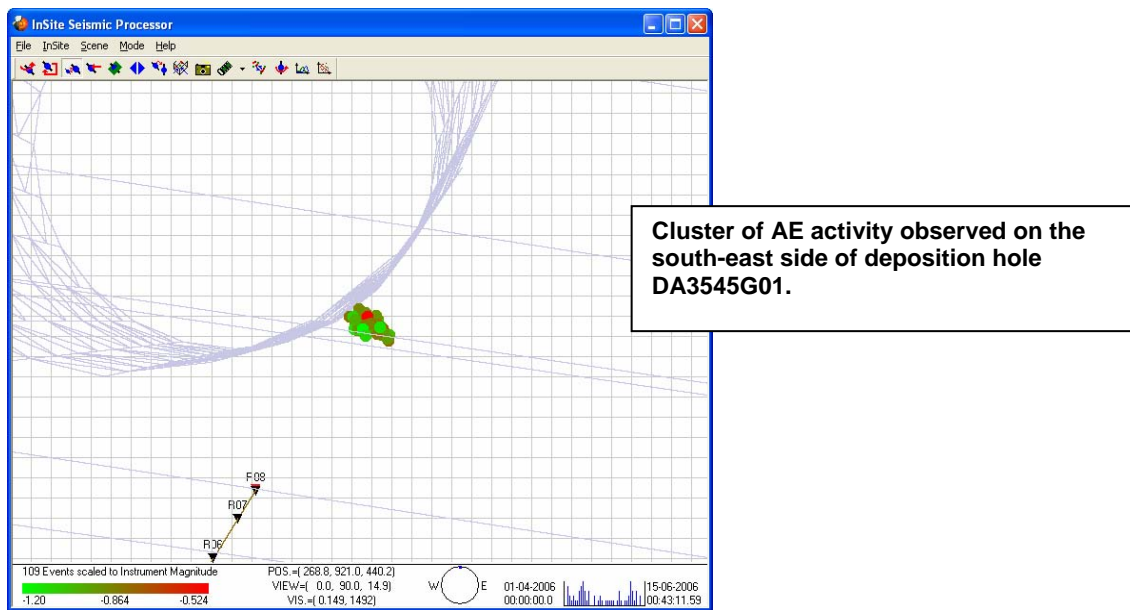
Sammanfattning

Experimentet Prototype Repository vid SKB:s Hard Rock Laboratory har designats för att simulera en deponeringstunnel i ett verkligt djupförvar för högaktivt radioaktivt avfall. Försöket består av en 90 m lång horisontell tunnel med en diameter på 5 m uttagen ur Äspödiorit. Försöket innehåller sex fullskaliga deponeringshål uttagna vertikalt från tunnels golv.

Denna rapport beskriver resultaten från acoustic emission (AE) och ultraljudsmätningar runt deponeringshål DA3545G01 i prototypförvaret. Syftet med mätningen är att undersöka förändringar i bergmassan som orsakats av en experimentell förvarsmiljö, speciellt med avseende på värmespänning från uppvärmning av kapseln och porttryck orsakade av förseglingen av tunneln. Denna rapport hänför sig till mätningar under perioden 1 april, 2006 till 30 september, 2006 och är den tredje rapporten med processning och tolkning av data från testerna. Ultraljudsmätningar har utförts i projektet Prototype Repository sedan september 1999. Mätningar gjordes runt de båda deponeringshålen i sektion 2 under borrningen av hålen. Syftet med dessa mätningar var att beskriva zoner med spänningsrelaterade sprickor och kvantitativt mäta sprickutbildningen i den störda zonen runt deponeringshålen. Ett permanent ultraljudssystem installerades i berget runt deponeringshål DA3545G01 i juni 2002.

Ultraljudsmätning används också för att 'aktivt' undersöka berget. Hastighetsförändringar mäts mellan sändare - givare par genom att använda en kors-korrelationsteknik som möjliggör en mätnoggrannhet på $\pm 2 \text{ ms}^{-1}$. Förändringar i amplitud och hastighet hos signalen när den passerat genom bergmassan i olika signalvägar relativt deponeringshålen, ("ray path") har sedan använts för att undersöka förändringar i bergegenskaperna. Hastigheterna användas för att bestämma förändringar i dynamisk modul, elasticitetsmodul och tvärkontraktionstal som ger direkta indikationer på egenskaperna på berget genom vilket vågen passerar. Sprickdensitet och vattenmättnadsgrad kan också beräknas för att fastställa förändringar i sprickornas egenskaper i den skadade och störda zonen. Mycket små förändringar i hastigheten hos P- och S-vågorna uppmättes under denna mätperiod. Trenden är att medelhastigheterna för P- och S-vågorna (uppmätt mellan alla par av sändare-givare) ökar under mätperioden, P-vågen med $1,25 \text{ ms}^{-1}$ och S-vågen med $0,70 \text{ ms}^{-1}$. Stora förändringar i hastighet observeras för några individuella signalvägar. Amplituderna på P- och S-vågorna minskar under den första månaden för att sedan öka under resten av mätperioden. Förändringarna i amplitud är mindre för denna period i jämförelse med tidigare perioder.

Förändringar i E-modul, tvärkontraktionstal, sprickdensitet och vattenmättnadsgrad har beräknats med hjälp av medelhastigheter för olika kategorier av signalvägar. Vattenmättnadsgraden ökar för signalvägar som går genom regioner med låga kompressionsspänningar eller dragspänningar och genom möjliga regioner med dragsprickor. Denna ökning kan vara ett resultat av den långsamma ökningen i tryck som kan trycka vätska in i sprickor från deponeringshålet. Generellt har mätningarna av hastighet och amplitud under denna sexmånaders period visat att bergvolymen runt deponeringshålet inte förändrats signifikant. En gradvis ökning av temperatur och tryck har lett till en långsam ökning av bergets styvhet samtidigt med en minskning i mängden sprickor. Under en period med relativt stabila förhållanden har inga dramatiska förändringar i bergmassan observerats.



Under sexmånadsperioden har 122 akustiska utstrålningar (AE) lokaliserats med stor säkerhet mha 151 ”triggade” händelser. Toppar i aktiviteter, under vilka 4 ”triggningar” observeras under en dag, har uppmätts två gånger nämligen den 18 april och den 3 juni. En kurva med ackumulerade ”triggade” händelser visar att hastigheten av ”triggningar” förblir tämligen konstant. I medeltal observerades 0.98 ”triggningar” per dag. Antalet lokaliserade händelser i medeltal per dag är 0.80 vilket är en ökning jämfört med de senaste 18 månaderna. Studie av den rumsliga fördelningen av AE visar att 109 av de 122 lokaliserade händelserna ligger i ett mycket begränsat kluster på djupet mellan 455,1 och 455,2 m på sydöstra sidan av deponeringshålet DA3545G01. Klustret ligger i en region med låga kompressionspänningar eller dragspänningar. Händelserna ligger så nära varandra så de kan anses ha uppstått vid samma diskontinuitet och de uppträder över hela rapporteringsperioden utan några pikar i aktivitet. AE kan ha uppstått i denna position p.g.a. tidigare, under uttaget av berget uppkomna mikrosprickor. En annan möjlighet är att de uppstått som ett resultat av rörelser i instrumentpositioner på deponeringshålets vägg.

Under det senaste året har en stor del av händelserna lokaliserats i den lågkompressiva regionen i NV och SO kvadranten av berget runt deponeringshålet. Under uttaget av berget och under den initiala uppvärmningen var merparten av händelserna lokaliserad till NO och SV kvadranten. Dessa delar utsätts för ökade kompressionsspänningar. Små kluster observerades i de ortogonala regionerna med låga kompressionspänningar eller dragspänningar. Det är viktigt att påpeka att händelser som lokaliserats under denna rapporteringsperiod är konsistenta med tidigare resultat d.v.s. alla händelser ligger i regioner där tidigare observerats händelser. Händelserna kan därför tolkas som en fortsatt aktivitet i den störda zonen, och är skapade av rörelser i tidigare existerande mikrosprickor eller som ett resultat av utvidgning eller bildning of nya mikrosprickor i den störda zonen. Antalet händelser är relativt få och indikerar därför att bergvolymen runt deponeringshålen har förblivit stabil under denna sexmånadersperiod.

Contents

Executive summary	5
Sammanfattning	7
Contents	9
Table of Figures	11
Table of Tables	14
1 Introduction	15
2 Specific Objectives	17
3 Results	19
3.1 Ultrasonic surveys	19
3.2 Acoustic Emissions	32
4 Conclusions	39
4.1 Monitoring Between April and September 2006	39
4.2 Summary of Monitoring from the Heating and Pressurisation Phase	41
4.3 Recommendations	41
Appendix I Previous Monitoring at the Prototype Repository	57
Appendix II Methodology	59
Processing Procedure	62
Appendix III Processing Parameters	67

Table of Figures

Figure 1-1: Plan view of the experimental tunnels at the Äspö HRL and the location of the Prototype Repository. A schematic illustration of the final experimental set up is shown with canisters and bentonite clay buffer installed in the 1.75m diameter deposition holes. Note the entrance of the tunnel is towards the left. Graphics are modified from SKB[1999].	15
Figure 3-1: Temperature around deposition hole DA3545G01. The sensors are positioned mid-way up the deposition hole with different depths into the rock mass (see right-hand inset) [Goudarzi, 2006].	19
Figure 3-2: Total pressure in (a) the backfill over deposition hole DA3545G01; and (b) in the rock adjacent to deposition hole DA3545G01 [Goudarzi, 2006]. The position of the sensors is presented in the figure legend as distance down, angle around and distance from the axis of the deposition	21
Figure 3-3: Average P- and S- wave (a) velocity change and (b) amplitude change, for the reporting period. Temperature (TR6045) and total pressure (PB616) are displayed on the secondary axes.	22
Figure 3-4: Example plots of (a) raw waveform data points and (b) cross correlation windows for the raypath transmitter 5 to receiver 13 on 31 st August and 1 st September 2006. The second plot shows the reference survey from 8 th December 2004.	23
Figure 3-5: Interpretation of the ultrasonic results during excavation in terms of disturbed and damaged regions around the deposition hole. Zones of induced stress are inferred from elastic modelling and the σ_1 orientation. After Pettitt et al.[1999].	25
Figure 3-6: Velocity changes measured on ray path category 'S3' (Figure 3-5) for deposition hole DA3545G01. Ray paths shown are from a top transmitter to receivers with increasing depth: a) transmitter, $t_n=1$, receiver, $r_n=5$; b) $t_n=1$, $r_n=6$; c) $t_n=1$, $r_n=7$; d) $t_n=4$, $r_n=1$. Schematic diagrams in the right margin indicate the relative locations of transmitter (red) and receiver (gold). Temperature (TR6045) is displayed on the secondary axes.	26
Figure 3-7: Velocity changes measured on ray path category 'S1' (Figure 3-5) for deposition hole DA3545G01. Ray paths shown are from a top transmitter to receivers with increasing depth: a) transmitter, $t_n=7$, receiver, $r_n=5$; b) $t_n=7$, $r_n=6$; c) $t_n=7$, $r_n=7$; d) $t_n=7$, $r_n=8$. Schematic diagrams in the right margin indicate the relative locations of transmitter (red) and receiver (gold). Temperature (TR6045) is displayed on the secondary axes.	27
Figure 3-8: Velocity change plots of 5 raypath categories around deposition hole DA3545G01 for (a) P-waves and (b) S-waves. Temperature (TR6045) and total pressure (PB616) are displayed on the secondary axes.	28
Figure 3-9: Amplitude change plots of 5 raypath categories around deposition hole DA3545G01 for (a) P-waves and (b) S-waves. Temperature (TR6045) and total pressure (PB616) are displayed on the secondary axes.	29
Figure 3-10: Example plot of raw waveform data points for the raypath transmitter 5 to receiver 5 on 12 th and 13 th September 2006.	30

Figure 3-11: Changes in rock parameters during this reporting period for average P- and S-wave velocity values on different raypath orientations. (a) Young’s Modulus, (b) Poisson’s Ratio, (c) Crack Density and (d) Saturation. Raypath orientations are described in Figure 3-5. Temperature (TR6045) and total pressure (PB616) are displayed on the secondary axes.	31
Figure 3-12: Temporal response plot of (a) AE triggers and (b) located AEs; number per day on left axes and cumulative number right hand axes.	34
Figure 3-13: Three views of AE activity located around deposition holes DA3545G01 and DA3551G01. (Top: Oblique view looking North; Middle: Transverse view looking north; Bottom: Plan view).	35
Figure 3-14: Waveforms from selected events shown in relation to a transverse view of AE activity.	36
Figure 3-15: Close up plan view of the cluster of 109 events. The background grid is 0.1m in size.	37
Figure 3-16: Temporal response plot of located AEs in the identified cluster; number per day on left axes and cumulative number right hand axes.	37
Figure 3-17: Plan view of AEs located around deposition hole DA3545G01 during (a) the excavation phase, (b) the first monitoring phase during heating and (c) this reporting period. The red arrows mark the orientation of the principle stress.	38
Figure 4-1: P- and S-wave (a) velocity change and (b) amplitude change from the start of monitoring, plotted alongside temperature (TR6045) and pressure (PB616) measurements in deposition hole DA3545G01. The vertical blue lines differentiate between periods of similar environmental conditions (see Table 4-1).	45
Figure 4-2: Average P- and S-wave velocity change for raypaths on category ‘S1’ together with temperature (TR6045) and total pressure (PB616) (top), Young’s Modulus and Poisson’s Ratio change (middle), and Crack Density and Saturation change (bottom).	46
Figure 4-3: Average P- and S-wave velocity change for raypaths on category ‘S3’ together with temperature (TR6045) and total pressure (PB616) (top), Young’s Modulus and Poisson’s Ratio change (middle), and Crack Density and Saturation change (bottom).	47
Figure 4-4: Average P- and S-wave velocity change for raypaths on category ‘C1’ together with temperature (TR6045) and total pressure (PB616) (top), Young’s Modulus and Poisson’s Ratio change (middle), and Crack Density and Saturation change (bottom).	48
Figure 4-5: Average P- and S-wave velocity change for raypaths on category ‘C2’ together with temperature (TR6045) and total pressure (PB616) (top), Young’s Modulus and Poisson’s Ratio change (middle), and Crack Density and Saturation change (bottom).	49
Figure 4-6: Average P- and S-wave velocity change for raypaths on category ‘Far’ together with temperature (TR6045) and total pressure (PB616) (top), Young’s Modulus and Poisson’s Ratio change (middle), and Crack Density and Saturation change (bottom).	50
Figure 4-7: Projections of all AEs located during the heating phase. Events are scaled to location magnitude.	51

Figure 4-8: (a) Number and cumulative number of located events from the start of monitoring, (b) average number of AE events per day (averaged over 17 days) and (c) temperature (TR6045) and pressure (PB616) measurements in deposition hole DA3545G01.	52
Figure 4-9: Schematic diagram of the deposition hole and explanation of changes experienced during Period 1.	53
Figure 4-10: Schematic diagram of the deposition hole and explanation of changes experienced during Period 2.	53
Figure 4-11: Schematic diagram of the deposition hole and explanation of changes experienced during Period 3.	54
Figure 4-12: Schematic diagram of the deposition hole and explanation of changes experienced during Period 4.	54
Figure 4-13: Top: Schematic diagram of the locations of all transducers on a single frame. Left: Photo of a section of the transducer assembly. Right: The transducer assembly during installation.	59
Figure 4-14: Plan view of the array geometry for Deposition Hole DA3545G01 during heating in the Prototype Tunnel. The blue solid lines represent direct raypaths between sondes illustrating their ‘skimming’ nature. The blue dashed line represents a raypath that travels through the deposition hole.	61
Figure 4-15: Schematic diagram of the hardware used for the heating stage in the Prototype Repository. The ultrasonic pulse generator sends a signal to each transmitter and the resulting signal is recorded on each receiver. The receivers are also used to listen for AE activity. The archive PC is required to make a copy of the data for backup purposes.	61
Figure 4-16: Waveforms recorded from one transmitter on the array of sixteen receivers. The gold markers indicate the transmission time. The blue and green markers indicate picked P- and S-wave arrivals respectively.	63
Figure 4-17: Locations of calibration shots obtained from a series of tests at 1 metre intervals down the wall of deposition hole DA3545G01. The two views show that these line up and are located close to the surface of the hole.	66
Figure 4-18: Example waveforms from each of the 16 receiving channels for a ‘pencil-lead break’ test undertaken against the Deposition Hole (DA3545G01) wall 6 metres below the tunnel floor.	66

Table of Tables

Table 3-1: Average number of located AEs per day for six monthly periods between 1 st October 2004 and 30 th September 2006.	32
Table 3-2: Values for the 109 events located in a cluster.	33
Table 4-1: Summary of velocity, amplitude and AE variation measured during four periods of temperature and/or pressure change.	42
Table 4-2: Summary of key interpretation of rock response from the ultrasonic measurements.	43
Table 4-3: Summary of ultrasonic monitoring at the Prototype Repository to-date. Response Periods are defined in <i>Haycox et al.</i> [2006].	57
Table 4-4: Boreholes used for AE monitoring of deposition hole DA3545G01.	60

1 Introduction

This report describes results from acoustic emission (AE) and ultrasonic monitoring around a canister deposition hole (DA3545G01) in the Prototype Repository Experiment at SKB's Hard Rock Laboratory (HRL), Sweden. The monitoring aims to examine changes in the rock mass caused by an experimental repository environment, in particular due to thermal stresses induced from canister heating and pore pressures induced from tunnel sealing. Monitoring of this volume has previously been performed during excavation [Pettitt *et al.*, 1999], and during stages of canister heating and tunnel pressurisation [Haycox *et al.*, 2005a,b; Haycox *et al.*, 2006]. Further information on this monitoring can be found in Appendix I. This report relates to the period between 1st April 2006 and 30th September 2006, and is the third of an ongoing 6-monthly processing and interpretation of the results for the experiment.

The Prototype Repository Experiment (Figure 1-1) has been designed to simulate a disposal tunnel in a real deep repository for disposal of high-level radioactive waste. Its objective is 'to test and demonstrate the integrated function of the repository components under realistic conditions on a full scale and to compare results with models and assumptions'. The experiment consists of a 90m long, 5m diameter sub-horizontal tunnel excavated in a dioritic granite using a Tunnel Boring Machine (TBM). The rock mass has two main discontinuous sets of sparse, en-echelon fractures [Patel *et al.*, 1997]. The Prototype Repository design incorporates six full-scale canister deposition holes which have been excavated vertically into the floor of the tunnel using a TBM converted to vertical boring. Each deposition hole measures 1.75m in diameter and approximately 8.8m in length. Simulated waste canisters, encased in a bentonite buffer, have been placed into each deposition hole and heated from within by specially designed electric heaters to simulate disposed radioactive material at elevated temperatures. The tunnel was then backfilled using a mixture of bentonite and crushed rock, and sealed using concrete plugs. A range of measurements are made in and around the tunnel and deposition holes.

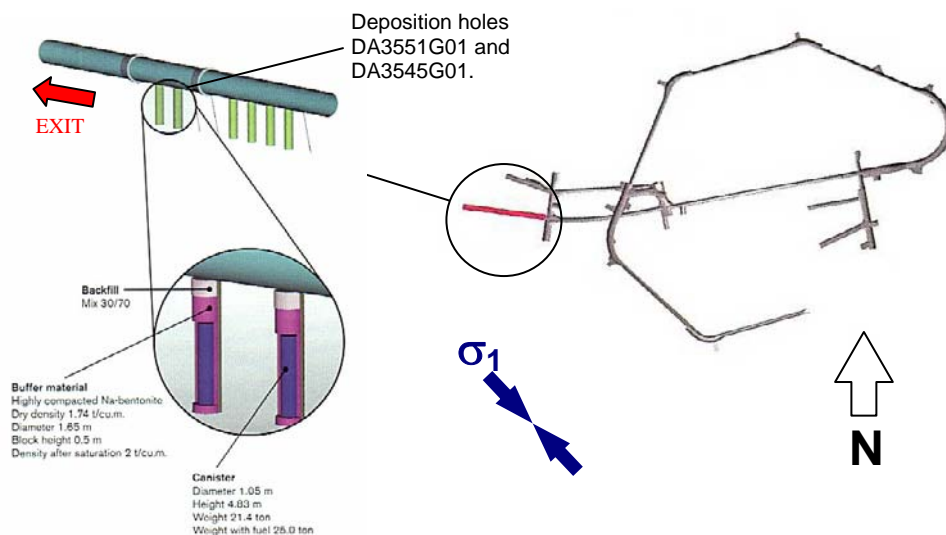


Figure 1-1: Plan view of the experimental tunnels at the Äspö HRL and the location of the Prototype Repository. A schematic illustration of the final experimental set up is shown with canisters and bentonite clay buffer installed in the 1.75m diameter deposition holes. Note the entrance of the tunnel is towards the left. Graphics are modified from SKB[1999].

AE and ultrasonic monitoring is a tool for remotely examining the extent and severity of damage and disturbance around an excavation. This can be induced by the excavation method itself; by the redistribution of stresses (loading or unloading) resulting from the void or by environmental affects such as heating, saturation or pressurisation. Acoustic techniques are particularly adept at assessing the Excavation Damaged or Disturbed Zone (EDZ) as they allow it to be mapped spatially and temporally with high resolution, and they allow the effect on the rock mass to be quantifiably measured. Furthermore, acoustic techniques allow investigations to be conducted remotely, without the need for potentially damaging coring. *Young and Pettitt*[2000] give a review of AE and ultrasonic results from a number of experiments conducted in different underground environments.

- AE monitoring is a ‘passive’ technique similar to earthquake monitoring but on a much smaller distance scale (source dimensions of millimetres). AEs occur on fractures in the rock sample when they are created or when they move. The data acquisition system triggers on AEs when they occur and records full-waveform information that can then be used to delineate the amount, time, location and mechanism of fracturing.
- Ultrasonic surveys are used to ‘actively’ examine the rock. In this case an array of transmitters sends signals to an array of receivers. Amplitude and velocity changes on the ray paths can be interpreted in terms of changes in the material properties of the rock. Calculations using the velocities can determine changes in dynamic moduli, Young’s modulus and Poisson’s ratio, to give direct indications of the properties of the rock through which the raypaths travel. Crack density and saturation can also be calculated to determine changes in crack properties in the damaged and disturbed zones.

Appendix II provides detailed descriptions of the data acquisition and processing used during this, and previous, monitoring periods. The ultrasonic array consists of twenty-four ultrasonic transducers configured as eight transmitters and sixteen receivers installed into four instrumentation boreholes using specially designed installation frames sealed within slightly expansive grout. The array is designed to provide good coverage for AE locations and provide ‘skimming’ ray paths so as to sample the rock immediately adjacent to the deposition hole wall. ASC’s InSite Seismic Processor [*Pettitt et al.*, 2005], has been used to automatically process both the AE and ultrasonic survey data. Appendix III A and Appendix III B give the processing parameters used. Data from daily ultrasonic surveys has been automatically picked and arrivals cross-correlated to a reference survey for high-precision measurements of P- and S-wave velocity change through the experiment. Arrivals of AEs have been manually picked and three dimensional source locations have been calculated.

2 Specific Objectives

This six-month period of ultrasonic monitoring in the Prototype Repository Experiment, has been undertaken with the following objectives:

- Produce accurate source locations for AEs so as to delineate the spatial and temporal extent of any brittle microcracking within the rock mass around the deposition hole and locate any movements on pre-existing macroscopic fractures.
- Conduct regular ultrasonic surveys to assess the effect of heating and other environmental changes on the velocity and amplitude of transmitted ultrasonic waves.
- Investigate changes in dynamic moduli and crack density to show how the properties of the rock volume around the deposition hole change through the experiment.
- Relate the AE and ultrasonic measurements to the measured *in situ* stress regime and other operating parameters such as temperature and fluid pressure.
- Outline how the results from this reporting period relate to previous monitoring periods, and into the overall experimental aims and objectives.

3 Results

3.1 Ultrasonic surveys

An indication of major environmental changes occurring in the tunnel and deposition holes can be ascertained from the temperature and pressure measurements. The temperature in the rock around the deposition hole is shown in Figure 3-1. All instruments show a slow increase in temperature over the six month time period. The increase for instrument TR6055, which has the highest temperatures, is from 53.1 to 54.2°C. This represents an increase of approximately 0.04°C per week.

Figure 3-2a shows total pressure in the tunnel backfill above the deposition hole. Pressure in the deposition hole is displayed in Figure 3-2b. A slow rate of increase is observed in pressure by the instruments in the backfill above the deposition hole. The maximum increase in pressure, of 0.127MPa, is recorded on instrument UFA16. The instruments located in the rock adjacent to the deposition hole (Figure 3-2b) also show a slow rate of increase over this period. PB616 experiences an increase from 5.74 to 6.40MPa. A similar increase is shown by instrument PB623 which increases from 3.90 to 4.68MPa. Instruments PB601 and UB610 show little change over this monitoring period.

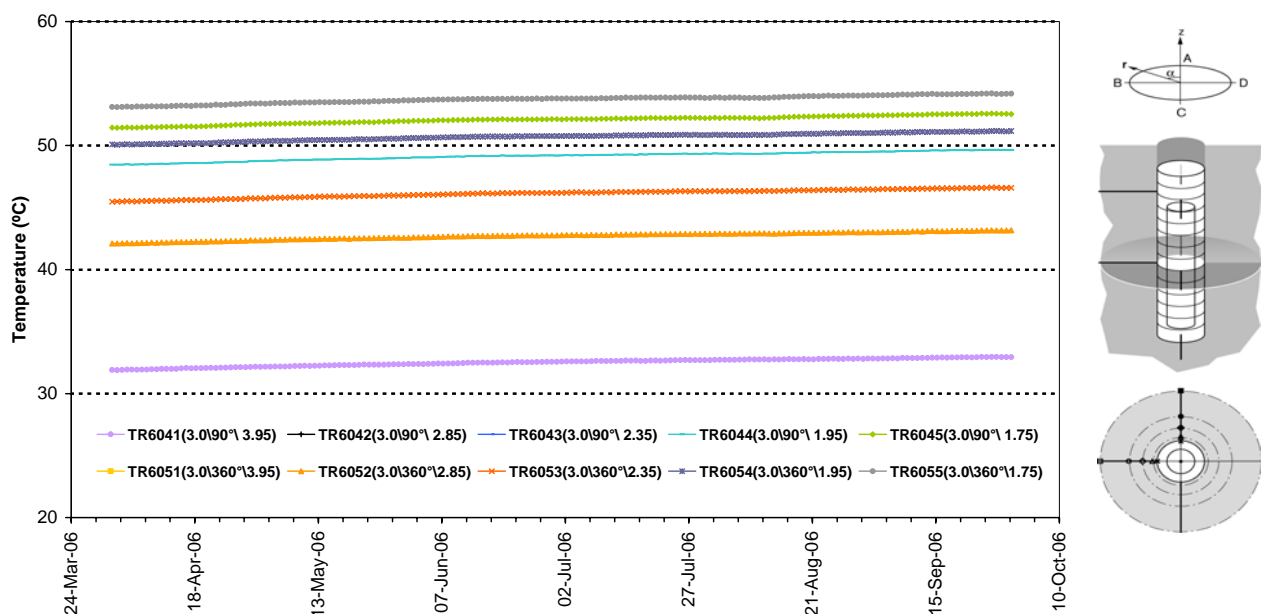


Figure 3-1: Temperature around deposition hole DA3545G01. The sensors are positioned mid-way up the deposition hole with different depths into the rock mass (see right-hand inset) [Goudarzi, 2006].

A problem with the ultrasonic data-acquisition system occurred between 13th June 2006 and 13th July 2006, which meant that no data was recorded. The problem was resolved through collaboration with SKB staff and acquisition has been successful for the remainder of the period. During this time there were no sudden changes in temperature or pressure (see Figure 3-1 to Figure 3-3), so no key ultrasonic response is likely to have been missed. The mean absolute P-wave velocity change between these dates is

0.43m.s⁻¹. On 52 of the 84 raypaths recorded, no change in velocity is measured between the dates. The downtime therefore has only had limited effect on the results and no bearing on the interpretations presented in this report.

Velocity changes are measured between transmitter-receiver pairs on the daily ultrasonic surveys using a cross-correlation technique that allows a velocity resolution of $\pm 2\text{m.s}^{-1}$. The reference survey for processing ultrasonic results for the previous monitoring periods, with manual P- and S-wave arrival picks, is recorded on 8th December 2004 [Haycox *et al.*, 2006]. Processing of data recorded during this monitoring period has used the same reference survey so that results can be accurately related to previous periods. Knowing the transmitter and receiver locations, the ultrasonic velocity for each ray path was calculated with an estimated uncertainty of $\pm 30\text{m.s}^{-1}$ (± 3 data points). A cross-correlation procedure was then used to automatically process subsequent surveys. This technique cross-correlates P- and S-wave arrivals from a transmitter-receiver pair with arrivals recorded on the same transmitter-receiver pair on the reference survey. This results in high-precision measurements of P- and S-wave velocity change, with estimated uncertainties of $\pm 2\text{m.s}^{-1}$ between surveys. The main reason for the reduction of uncertainty when using the cross-correlation procedure is the dependency of manual picking on the user's judgement of the point of arrival. This can usually be quite indiscriminate because of random noise superimposed on the first few data points of the first break. The cross-correlation procedure then allows for a high-resolution analysis to be performed and hence small changes in velocity to be observed. This is extremely important when changes in rock properties occur over only a small section (5%) of the ray path.

Average P- and S-wave velocity change is shown in Figure 3-3a. Little change in P- or S-wave velocity is measured in the first one and a half months of monitoring. Between 19th and 21st May P-wave velocity decreases by 0.45m.s⁻¹. A sudden increase in velocity occurs between 31st August and 1st September. P-wave velocity increases by 1.18m.s⁻¹ and S-wave velocity increases by 0.40m.s⁻¹. This is a relatively large change over one day, given that the average is determined from velocity measured on many raypaths. Similar observations have been noted in previous monitoring periods [Haycox *et al.*, 2005b; Haycox *et al.*, 2006]. Figure 3-4 shows an example of the waveform records. An increase in velocity is represented by a movement in the waveform to the left. After the sudden rise, both P- and S-waves remain constant, so that by the end of the reporting period average velocity is 1.25m.s⁻¹ faster for P-wave and 0.70m.s⁻¹ faster for S-wave, than at the start.

As in previous observations of similar velocity changes to that observed on 31st August, not all ray paths are affected in an identical manner, nor are ray paths purely from one instrumentation borehole to another affected. Consequently this change has been interpreted as a localised change in the general rock properties rather than a systematic change in the measurement devices used in the project (the records would be expected to respond identically if the observation was due to the acquisition system behaviour). Further discussion of previous similar changes can be found in Section 5 of the previous report (Haycox *et al.*[2006]).

Average amplitude changes measured during this reporting period are presented in Figure 3-3b. In the first month, P- and S-wave amplitudes decrease, reaching -0.11 and -0.07dB respectively by 30th April 2006. After this date amplitude increases at a relatively constant rate, with S-wave amplitude increasing marginally more than the P-wave amplitude. By the end of this reporting period P-wave amplitude is approximately 0.14dB

higher than at the start, and S-wave amplitude is 0.18dB higher than at the start. The changes in amplitude are less than were recorded during the previous six month reporting period, when both P- and S-wave amplitude decreased, and then increased by over 0.5dB. A discussion of changes throughout the monitoring is carried out in Section 4.2.

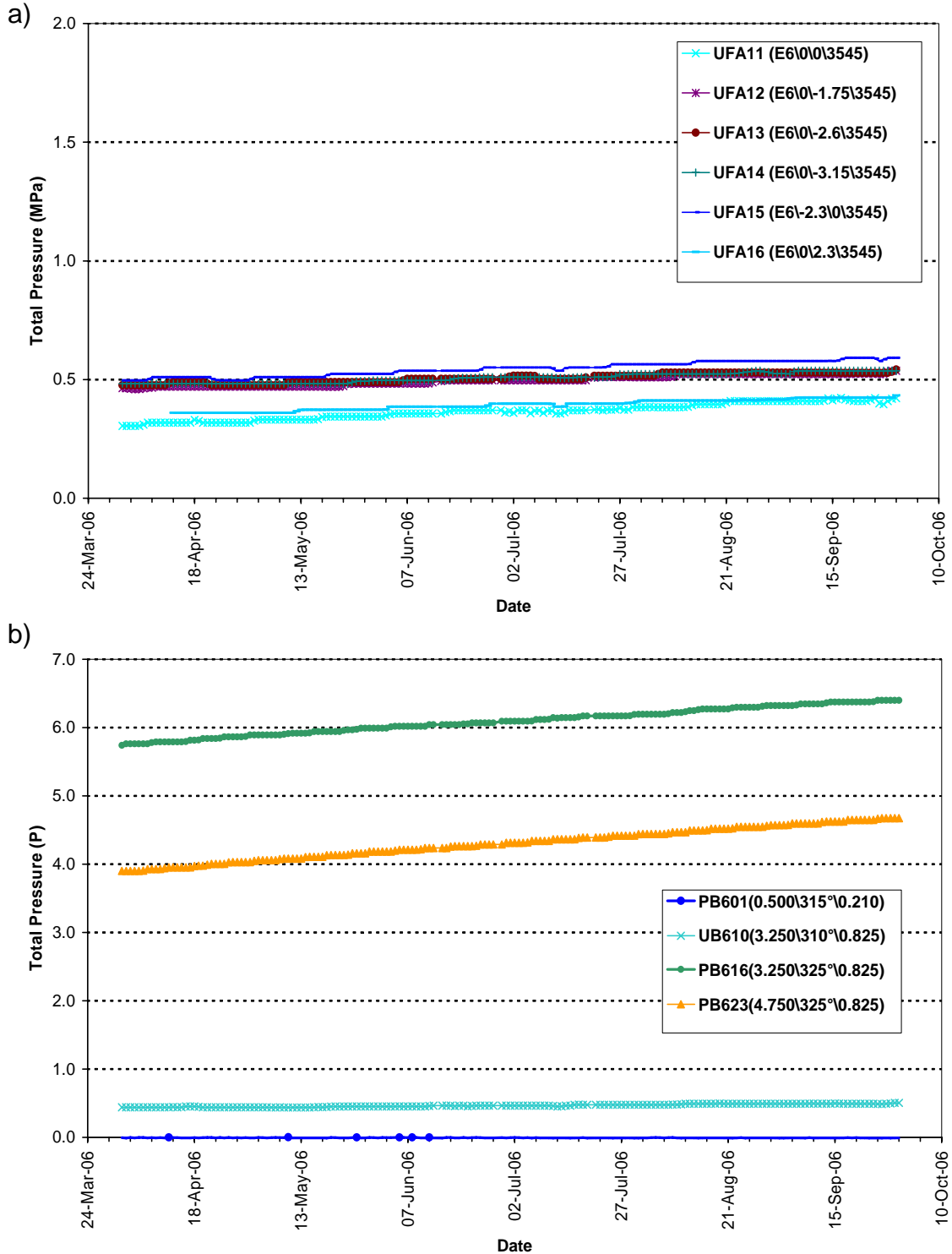


Figure 3-2: Total pressure in (a) the backfill over deposition hole DA3545G01; and (b) in the rock adjacent to deposition hole DA3545G01 [Goudarzi, 2006]. The position of the sensors is presented in the figure legend as distance down, angle around and distance from the axis of the deposition

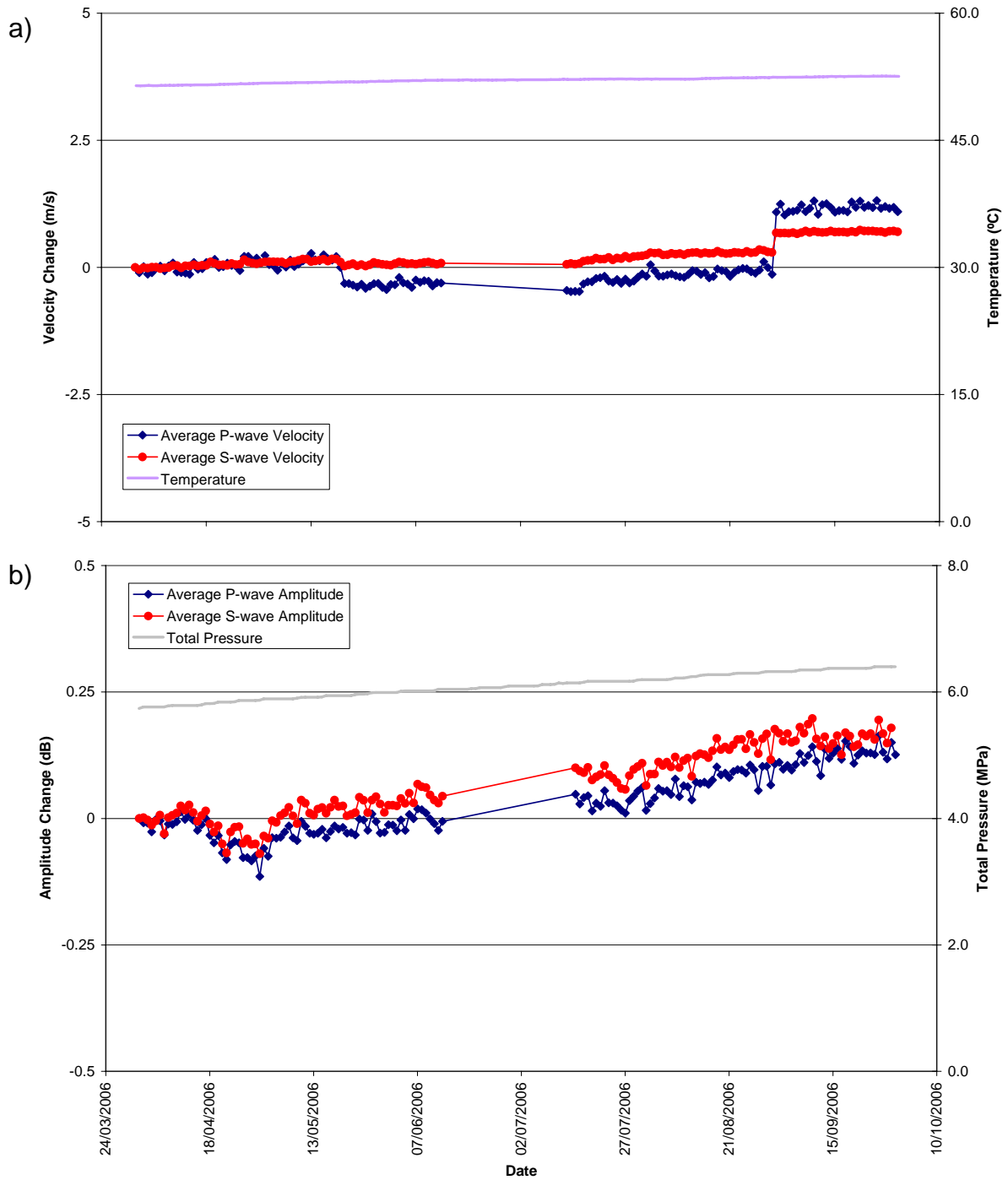


Figure 3-3: Average P- and S- wave (a) velocity change and (b) amplitude change, for the reporting period. Temperature (TR6045) and total pressure (PB616) are displayed on the secondary axes.

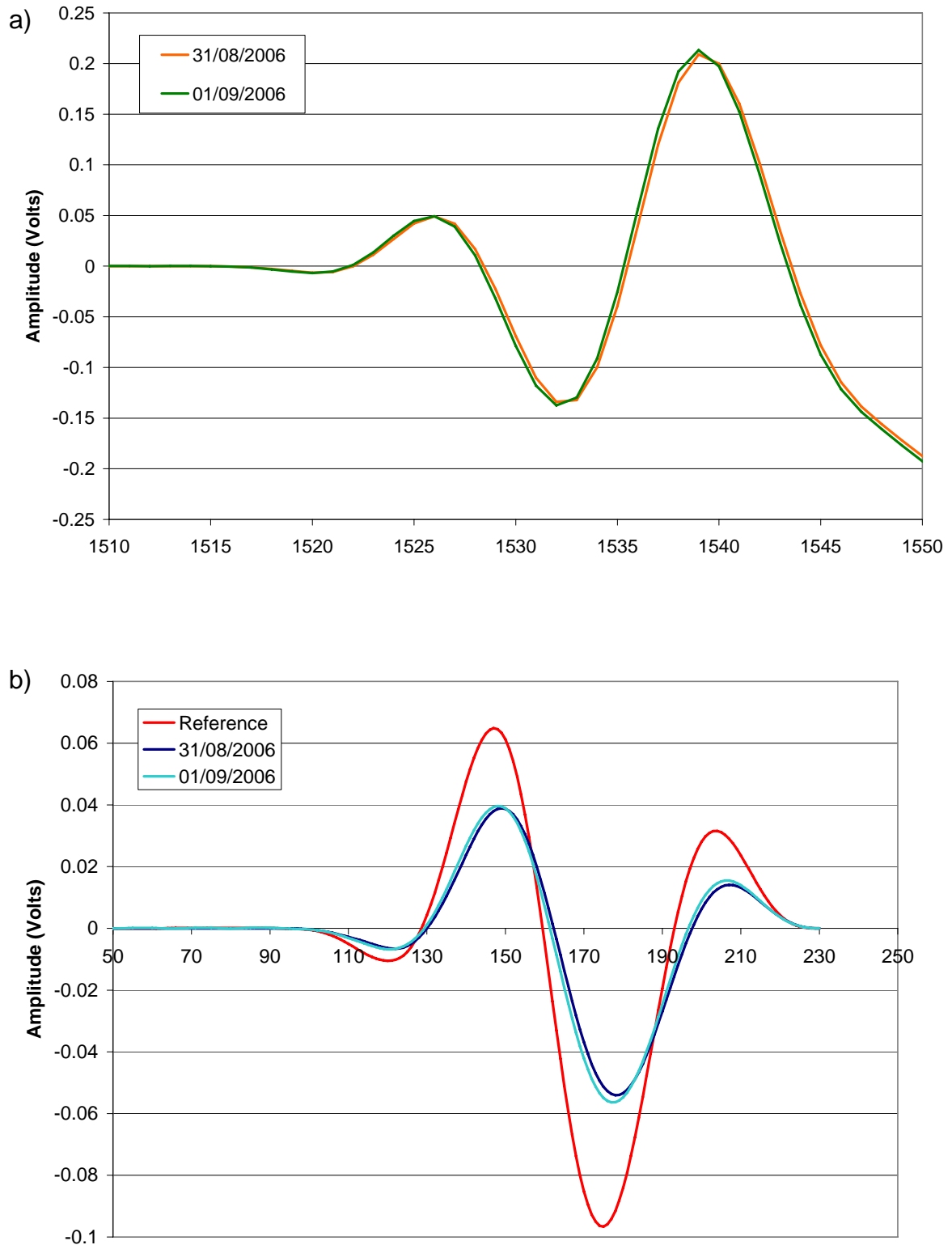


Figure 3-4: Example plots of (a) raw waveform data points and (b) cross correlation windows for the raypath transmitter 5 to receiver 13 on 31st August and 1st September 2006. The second plot shows the reference survey from 8th December 2004.

Pettitt et al.[1999] categorised raypaths from ultrasonic surveys into six types depending on their orientation with respect to the deposition hole and the in situ stress field (Figure 3-5). This figure shows an interpretation of the ultrasonic results in terms of disturbed and damaged regions around the void during the excavation phase of the experiment. *Pettitt et al.*[2000] undertook three-dimensional elastic stress modelling to describe these zones of stress.

Example raypaths from category 'S3' are presented in Figure 3-6. These raypaths pass within centimetres of the deposition hole through the excavation damaged zone, in a region of low compressive or tensile stress. These particular raypaths have been chosen because they provide a comparison of velocity changes down the length of the deposition hole. Each plot of velocity change is accompanied by a schematic diagram giving a perspective of the region through which the raypath passes. Very little velocity change is recorded on three of the raypaths. The only significant change is observed for P-wave velocity on raypath transmitter 1 to receiver 6. This remains at a constant P-wave velocity for the first two and a half months, but then increases by 15.1m.s^{-1} to the end of the reporting period. S-wave velocity does not significantly increase on this raypath; neither does it on the other raypaths chosen in this category.

Figure 3-7 shows velocity results for raypaths of category 'S1'. These raypaths pass through a region of high compressive stresses and permanent damage close to the deposition hole wall imaged by relatively high AE activity during excavation. During this period, very little change is observed in P- or S-wave velocity. The only significant increase is measured on transmitter 7 to receiver 6, in which P-wave velocity is shown to increase by a maximum of 4.1m.s^{-1} during the six months.

Figure 3-8 compares the results of average velocity change across different raypath categories described in Figure 3-5. P-wave velocity shows a greater change than S-wave velocity. Raypath category 'S3' exhibits the greatest variation. P-wave velocity gradually increases from July. By 31st August, P-wave velocity on this raypath category had increased by 1.38m.s^{-1} . After the velocity jump described earlier, velocity does not vary until the end of the reporting period. A decrease in velocity is observed on all categories between 19th and 22nd May 2006. This is a small change, but is recognisable in the data. Similar patterns are observed for S-wave velocity change, but the scale of change is smaller.

Figure 3-9 compares the results of average amplitude change across different raypath categories described in Figure 3-5. P- and S-wave amplitudes exhibit a similar pattern of change over the course of the reporting period. Before the start of May, amplitude remains the same and varies by no more than $\pm 0.13\text{dB}$. For the remaining five months, amplitude gradually increases. An interesting observation is the rapid increase in amplitude recorded on the P-wave of category 'C1' between 12th and 13th September 2006. This does not occur on any other category, for either P- or S-waves. The P-wave arrival on these two days, for an example raypath of this category, is plotted in Figure 3-10. The increase in P-wave amplitude occurs on 7 of the raypaths in the category.

Figure 3-11 shows changes in Young's Modulus, Poisson's Ratio, Crack Density and Saturation Parameters calculated from the average measured velocities for the raypath categories. 'Crack Density' and 'Saturation' of the rock mass are determined using the method of *Zimmerman and King*[1985], as described in Appendix II. In general, there is a gradual increase in Young's modulus over the period, indicating a stiffening of the rock mass.

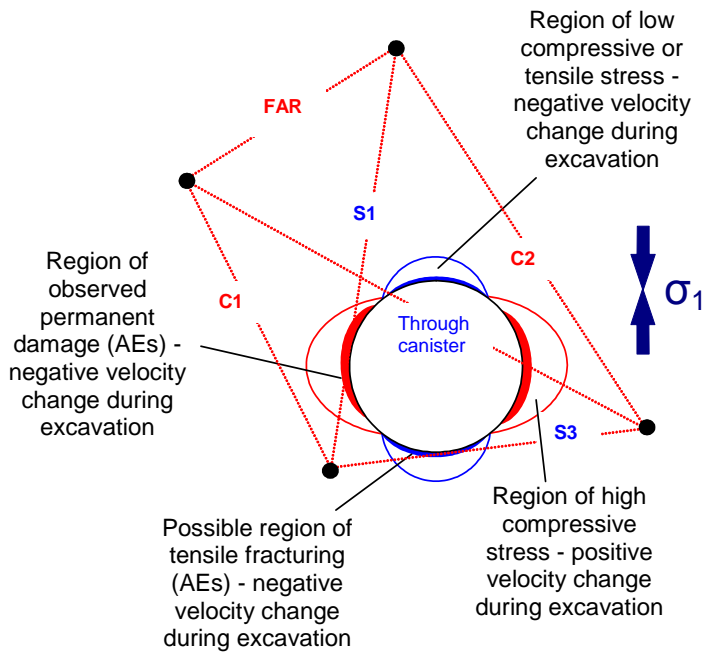


Figure 3-5: Interpretation of the ultrasonic results during excavation in terms of disturbed and damaged regions around the deposition hole. Zones of induced stress are inferred from elastic modelling and the σ_1 orientation. After Pettitt et al.[1999].

Saturation is observed to increase to a greater extent on category ‘S3’. These raypaths pass through the region of low compressive or tensile stress, and through a possible region of tensile fracturing. In previous monitoring periods, this category has been very susceptible to changes in temperature and pressure. This small increase may be a result of the slow increase in pressure that could be pressurising fluid into the cracks from the deposition hole.

The sudden increase in velocities between 12th and 13th September 2006 describe an increase in Young’s modulus indicating that the rock becomes stiffer. In this instance, the change does not coincide with rapid changes in pressure or temperature. This is interpreted as a relatively sudden adjustment in the rock mass overall leading to a general closure of cracks.

Overall during this six month period, the velocity and amplitude results have shown that the rock mass around the deposition hole has not altered significantly. Gradual increases in temperature and pressure have led to a slow stiffening of the rock, alongside a similarly slow reduction in crack density. During a relatively stable period of environmental characteristics, no dramatic changes in the rock mass have been measured.

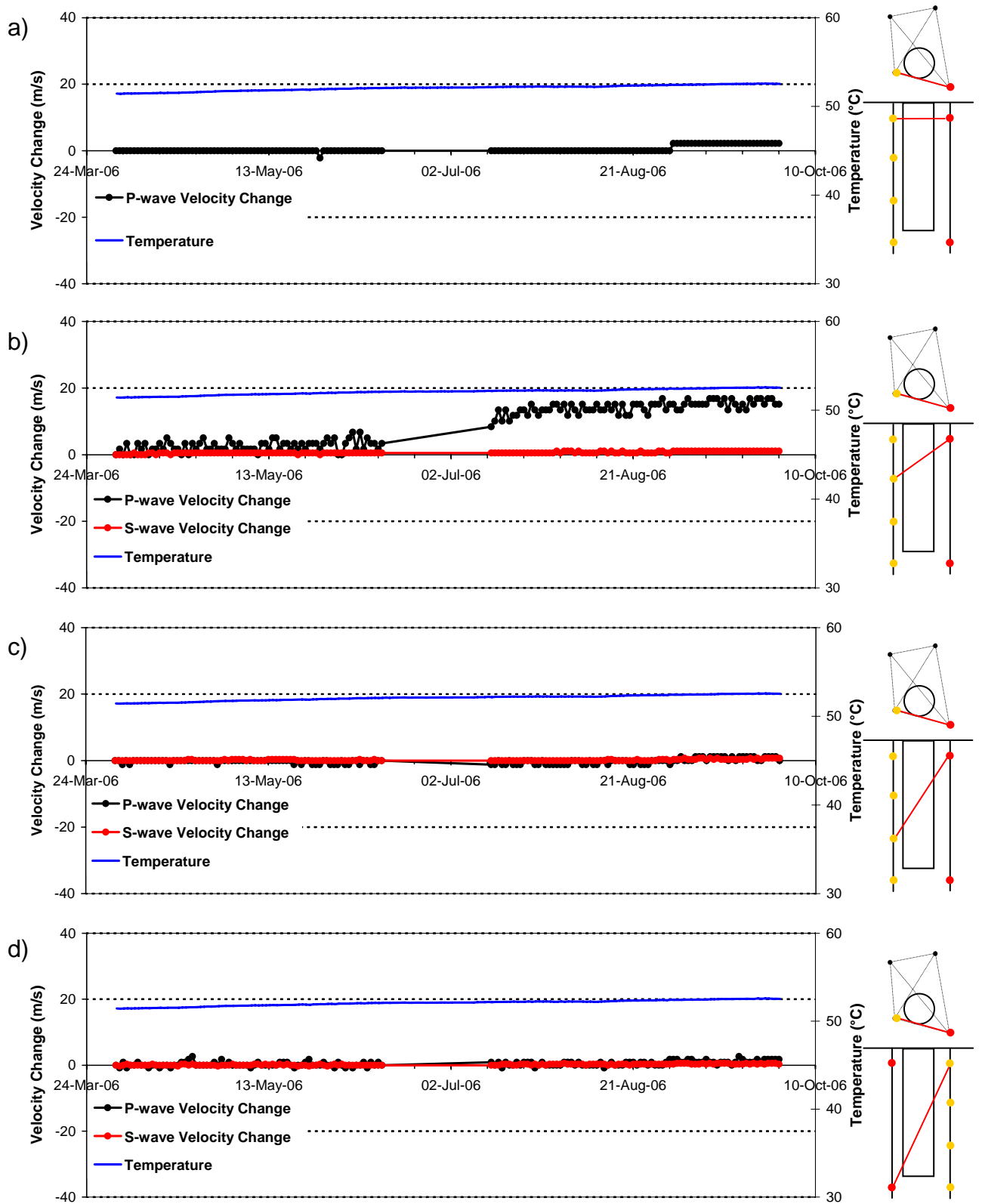


Figure 3-6: Velocity changes measured on ray path category 'S3' (Figure 3-5) for deposition hole DA3545G01. Ray paths shown are from a top transmitter to receivers with increasing depth: a) transmitter, $t_n=1$, receiver, $r_n=5$; b) $t_n=1$, $r_n=6$; c) $t_n=1$, $r_n=7$; d) $t_n=4$, $r_n=1$. Schematic diagrams in the right margin indicate the relative locations of transmitter (red) and receiver (gold). Temperature (TR6045) is displayed on the secondary axes.

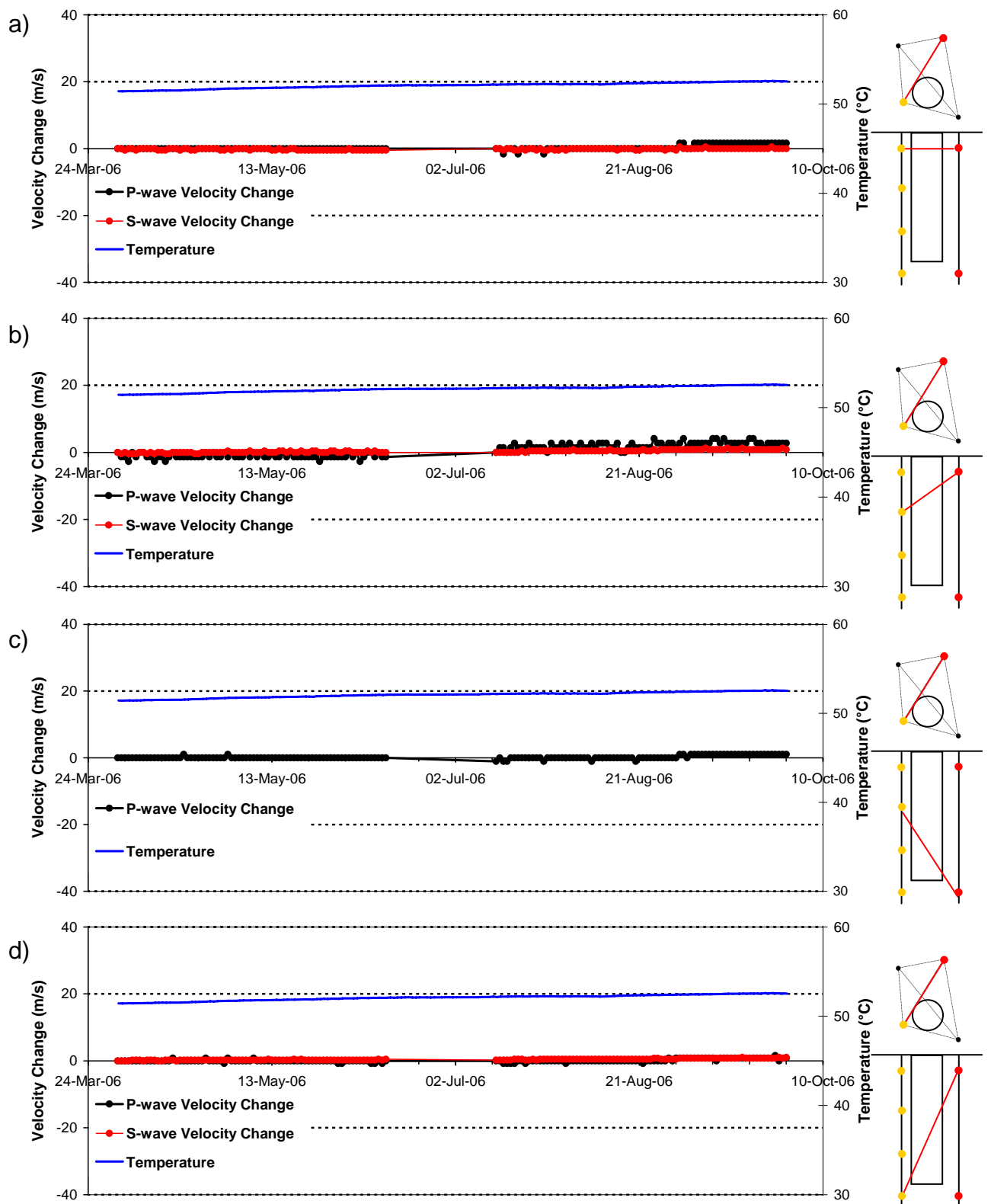


Figure 3-7: Velocity changes measured on ray path category 'S1' (Figure 3-5) for deposition hole DA3545G01. Ray paths shown are from a top transmitter to receivers with increasing depth: a) transmitter, $t_n=7$, receiver, $r_n=5$; b) $t_n=7$, $r_n=6$; c) $t_n=7$, $r_n=7$; d) $t_n=7$, $r_n=8$. Schematic diagrams in the right margin indicate the relative locations of transmitter (red) and receiver (gold). Temperature (TR6045) is displayed on the secondary axes.

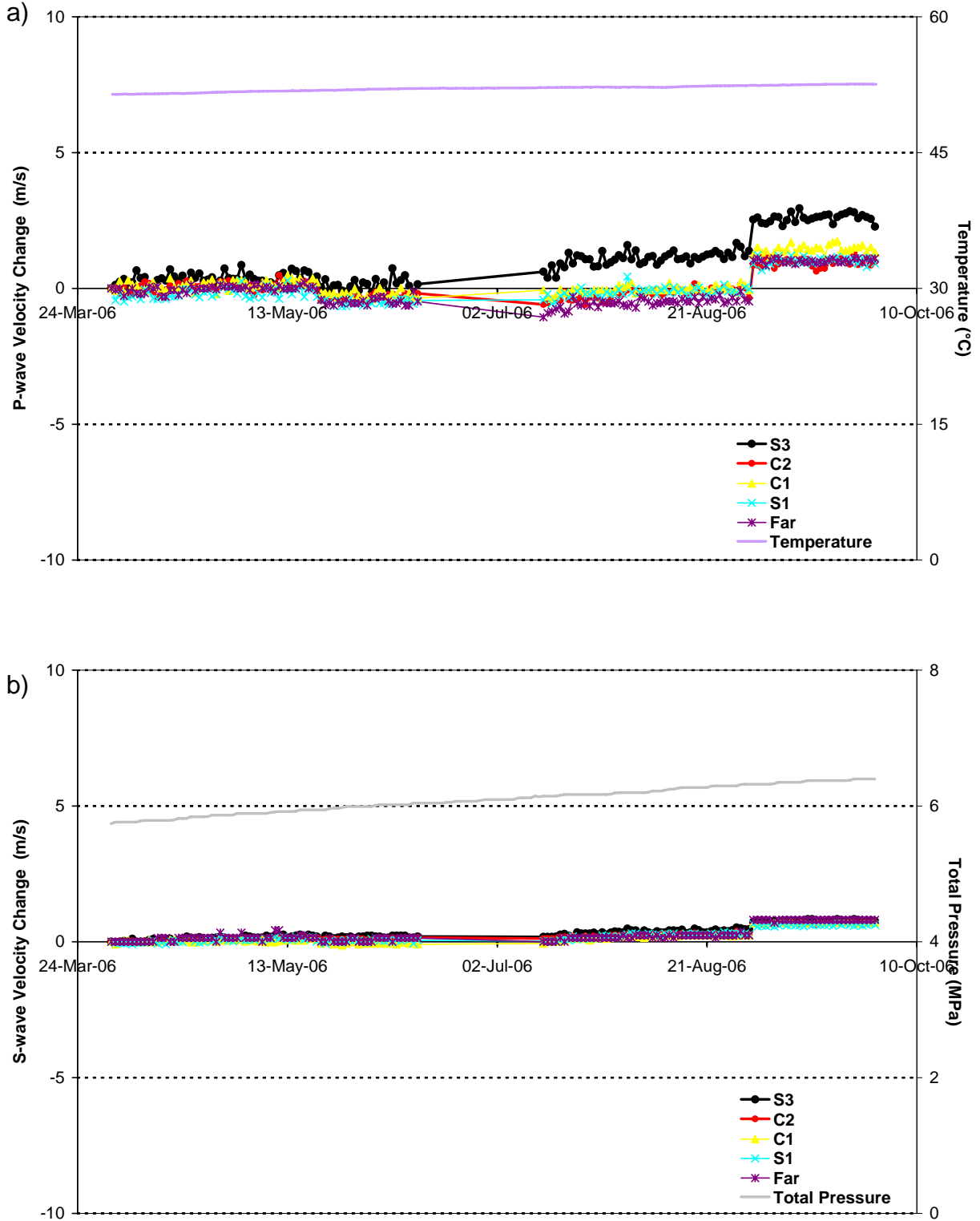


Figure 3-8: Velocity change plots of 5 raypath categories around deposition hole DA3545G01 for (a) P-waves and (b) S-waves. Temperature (TR6045) and total pressure (PB616) are displayed on the secondary axes.

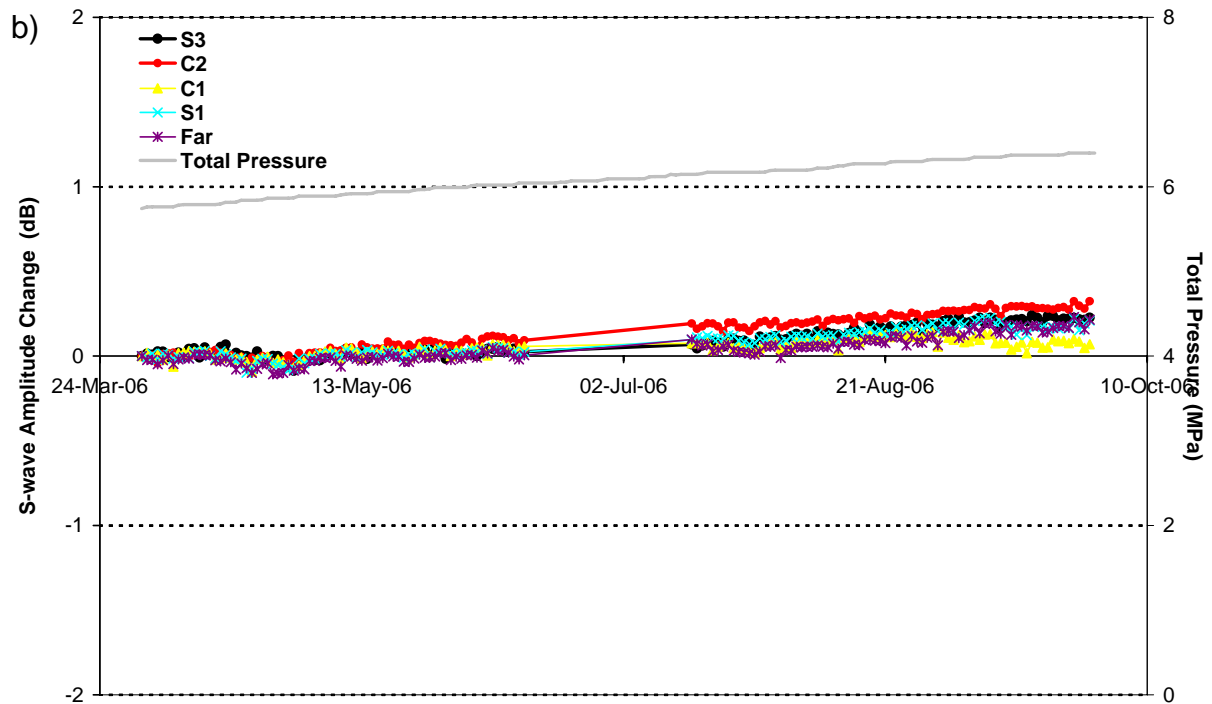
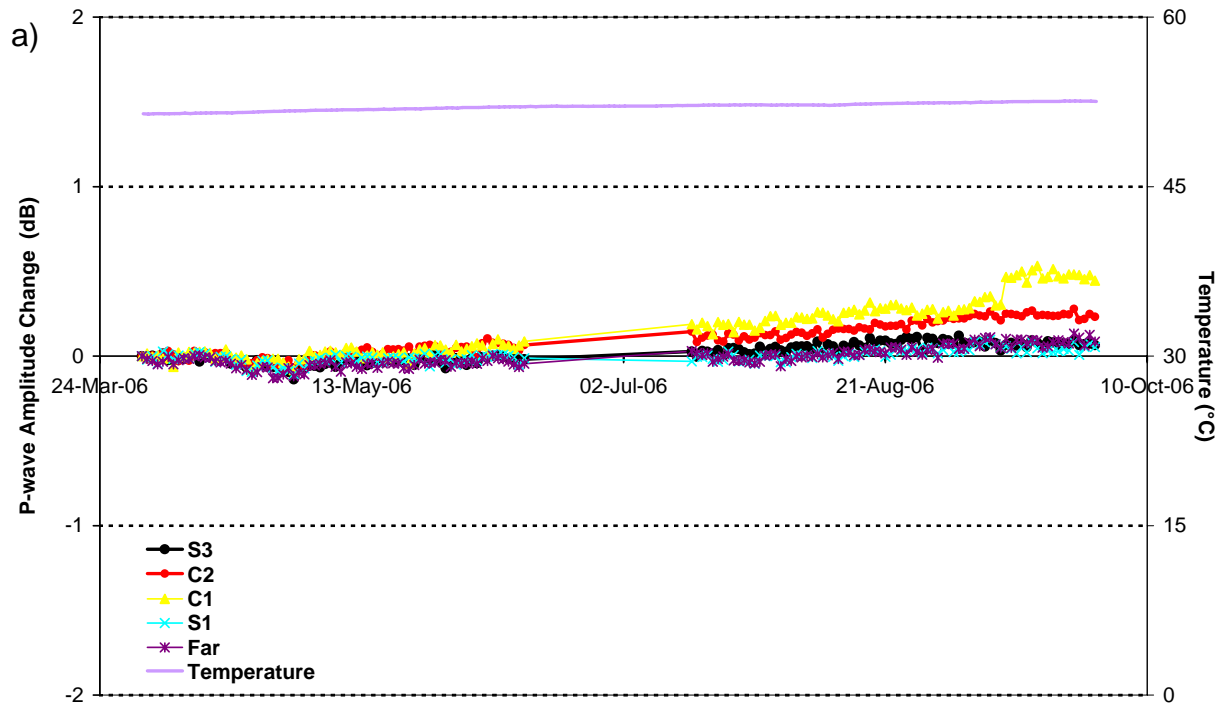


Figure 3-9: Amplitude change plots of 5 raypath categories around deposition hole DA3545G01 for (a) P-waves and (b) S-waves. Temperature (TR6045) and total pressure (PB616) are displayed on the secondary axes.

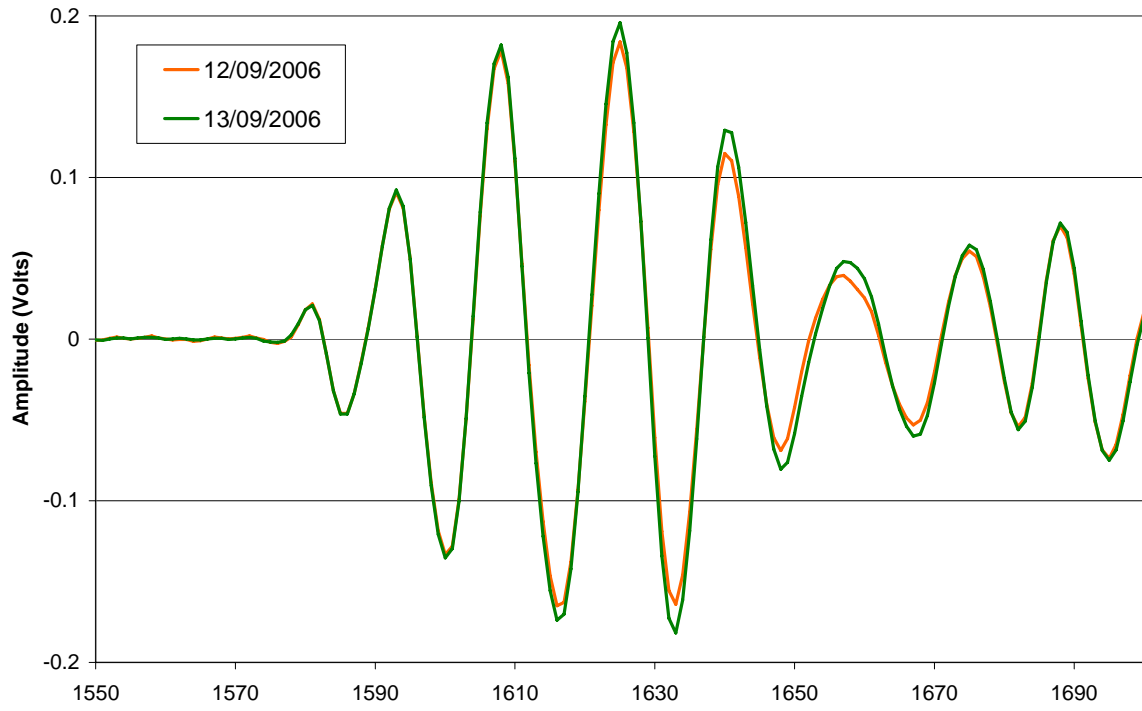


Figure 3-10: Example plot of raw waveform data points for the raypath transmitter 5 to receiver 5 on 12th and 13th September 2006.

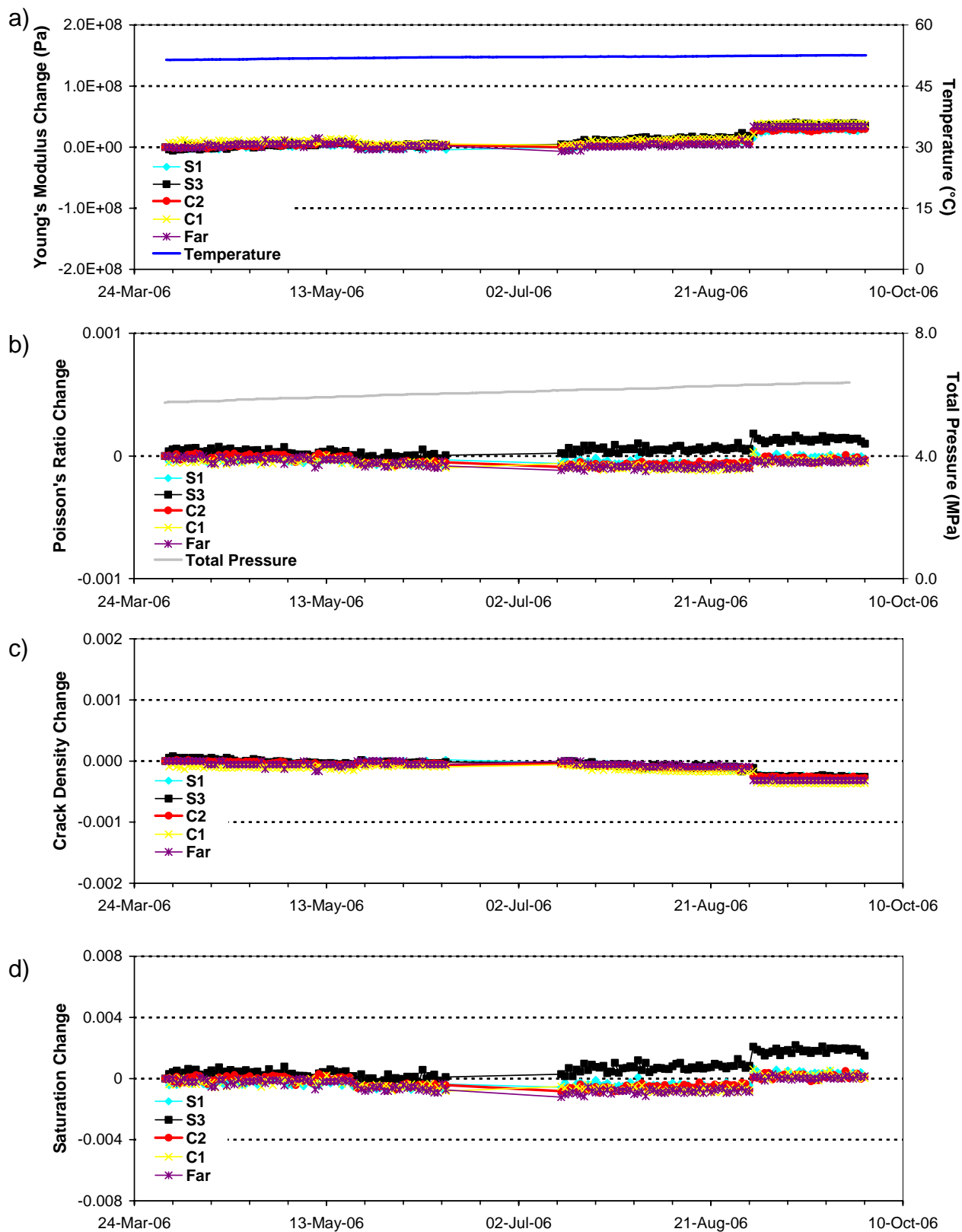


Figure 3-11: Changes in rock parameters during this reporting period for average P - and S -wave velocity values on different raypath orientations. (a) Young's Modulus, (b) Poisson's Ratio, (c) Crack Density and (d) Saturation. Raypath orientations are described in Figure 3-5. Temperature (TR6045) and total pressure (PB616) are displayed on the secondary axes.

3.2 Acoustic Emissions

Processing of acoustic emissions has been undertaken following the procedures outlined in Appendix II. 122 events have been located with high confidence from 151 triggered events during this reporting period. Note that the system was not operating between 13th June and 13th July 2006. The estimated uncertainties for these event are of the order 10cm, estimated using calibration ‘hits’ performed within the deposition holes after excavation (see Appendix II for further details).

The temporal response of triggers and located events recorded during this monitoring period is shown in Figure 3-12. A trigger is described as an event that has been acquired by the system, but may not be of sufficient energy or quality to be located during the processing procedure. ‘Noise’ events, produced from electrical or man-made sources, have been removed from this count to allow a more accurate representation of fracturing in the rock. The temporal distribution of AE triggers is shown in Figure 3-12a. Peaks, in which 4 triggers are recorded on one day, are observed twice on the 18th April and 3rd June. The cumulative plot shows that although the rate of triggers remains reasonably constant, the number of triggers in April is high with 40 recorded in 30 days (1.33 triggers per day), and also at the start of June with 18 recorded in 13 days (1.39 triggers per day). On average, 0.98 triggers were recorded per day. The temporal response of the 122 AEs (located events) is displayed in Figure 3-12b. A maximum of four events are located in a day on 18th April and on 3rd June (all triggers locate). An average of 0.80 events are located per day, an increase from the previous 18 months (Table 3-1).

Table 3-1: Average number of located AEs per day for six monthly periods between 1st October 2004 and 30th September 2006.

Time Period	Average Number of Events per Day
1 st October 2004 to 31 st March 2005	0.32
1 st April 2005 to 30 th September 2005	0.21
1 st October 2005 to 31 st March 2006	0.27
1 st April 2006 to 30 th September 2006	0.80

AEs have been visualised in the InSite Seismic Processor in relation to physical features of the Prototype Repository. Three projections are presented in Figure 3-13 showing the spatial distribution of located AEs. Instrumentation boreholes are represented by brown vertical lines and the tunnel and deposition hole outlines are represented by grey wireframes. The majority of the 122 located events locate in a very tight cluster at a depth of between 455.1 and 455.2m down deposition hole DA3545G01, on the SE side. This cluster of 109 events is indicated in Figure 3-13 by the pointer ‘i’. Haycox *et al.* [2006] observed 38 events locating in this position during the previous six month reporting period, representing 78% of events located in that period. Waveforms of selected events are presented in Figure 3-14. These show typical waveforms recorded on different sensors and demonstrate the high quality data that can be recorded using the array.

The cluster of 109 events locates in a region of low-compressive or tensile stresses. Analysis of these events, shows the average position of the events to be at (268.75, 921.08, 455.11). The range of values measured generally supports the accuracy of location measured by calibration hits (see Appendix II). The events are close enough together to be considered occurring on the same feature, as demonstrated by Figure 3-15 which shows a close up plan view of the events. The temporal response of these events is presented in Figure 3-16. AEs occur over the whole reporting period with no significant peaks in activity. Four events occur on 18th April and on 3rd June, as identified previously. AEs may be occurring at this position due to the presence of a pre-existing microcrack, generated during excavation. Alternatively, the events may result from movement of an instrument positioned on the deposition hole wall. Sensors are identified as being in this location by *Gourdazi and Johannesson*[2006], temperature sensor WB618T for example.

Table 3-2: Values for the 109 events located in a cluster.

	Northing (m)	Easting (m)	Depth (m)
Minimum	268.70	921.00	455.06
Maximum	268.82	921.16	455.17
Mean	268.75	921.08	455.11
Standard Deviation	0.02	0.04	0.02

Figure 3-17 shows plan views of events recorded during excavation, the first period of heating and this reporting period. The majority of the events located in the NE and SW quadrants during excavation and initial heating [*Pettitt et al.*, 2000; *Pettitt et al.*, 2002, *Haycox et al.*, 2005a]. These regions are subject to increased compressive stresses, as identified from the insitu stress field by *Pettitt et al.*[1999]. Smaller cluster were observed in the orthogonal regions of low-compressive or tensile stress. It is important to note that events located during this reporting period are consistent with previous results, i.e. no events are positioned in regions where activity has not been observed in the past. The events can therefore be interpreted as a continuation of activity in the damage zone, and are created either by movement on pre-existing microcracks, or as a result of extension or formation of new microcracks in the existing damaged region. The numbers of events are relatively low and therefore indicate the rock mass around the deposition holes has remained stable during this six-month period. For the past year, including this reporting period and the previous one presented by *Haycox et al.*[2006], a greater proportion of events have been locating in a tight cluster in the low-compressive region at a mean depth of 455.11m. This cluster should be the focus of further investigation.

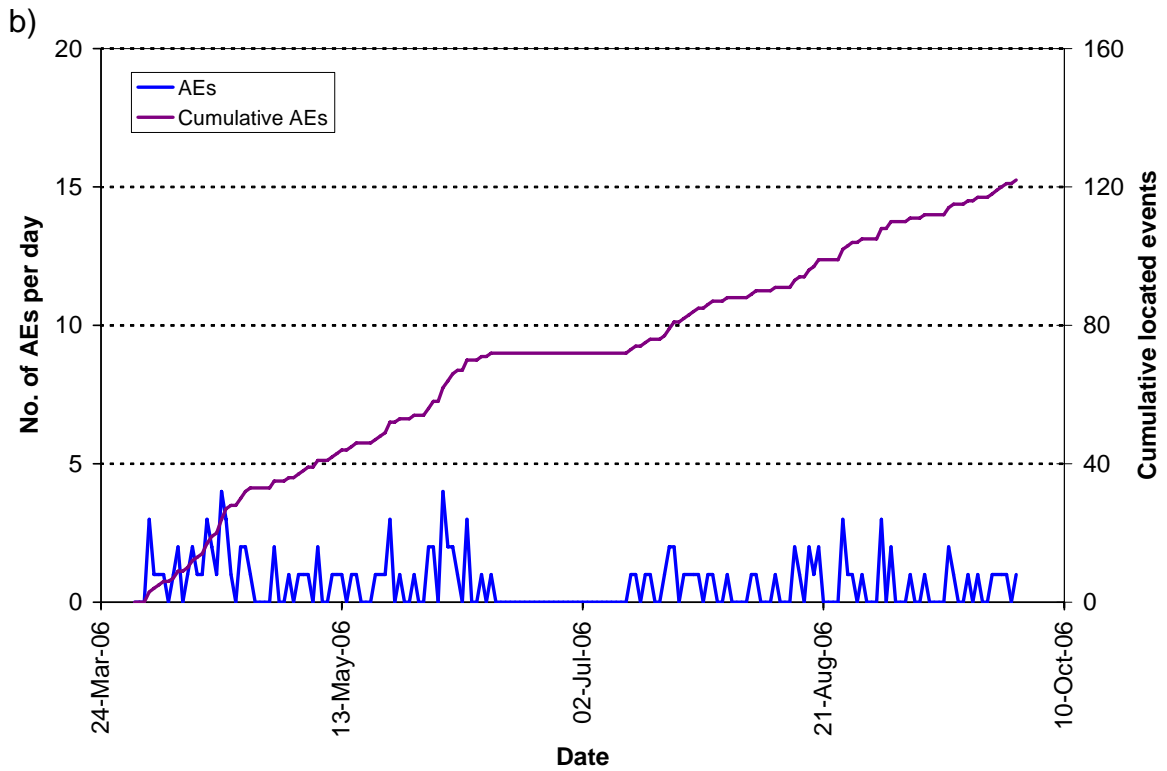
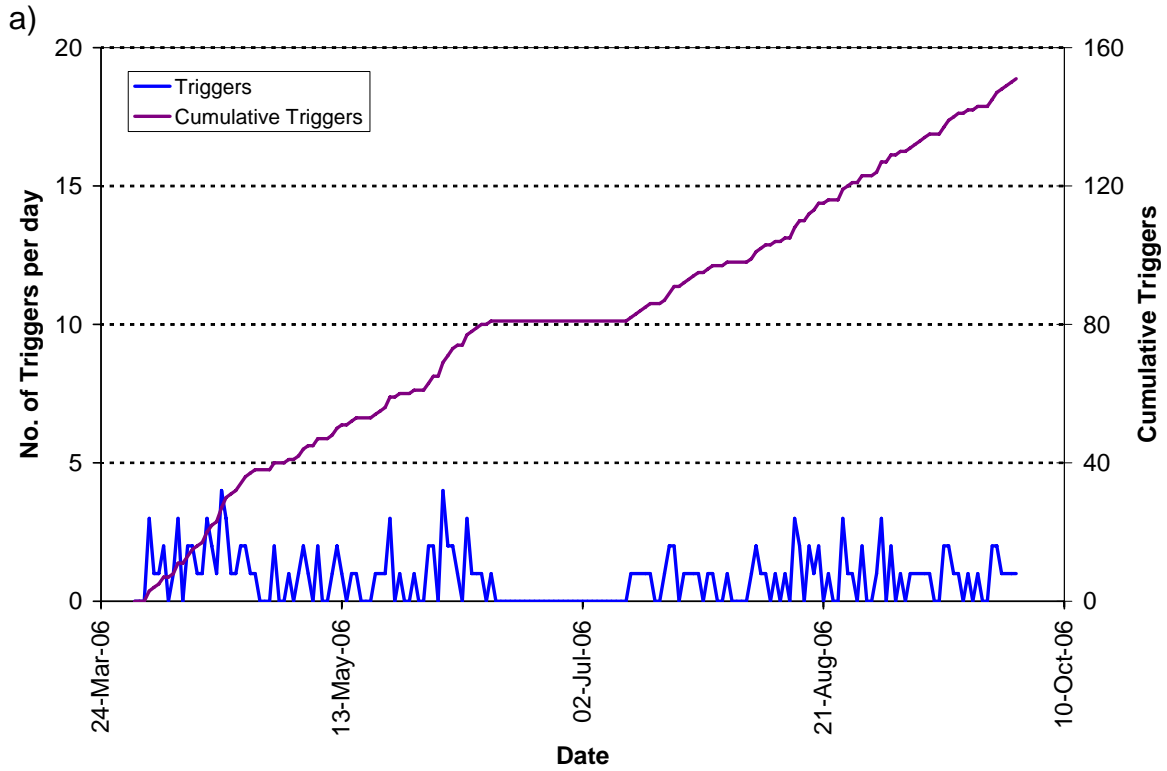


Figure 3-12: Temporal response plot of (a) AE triggers and (b) located AEs; number per day on left axes and cumulative number right hand axes.

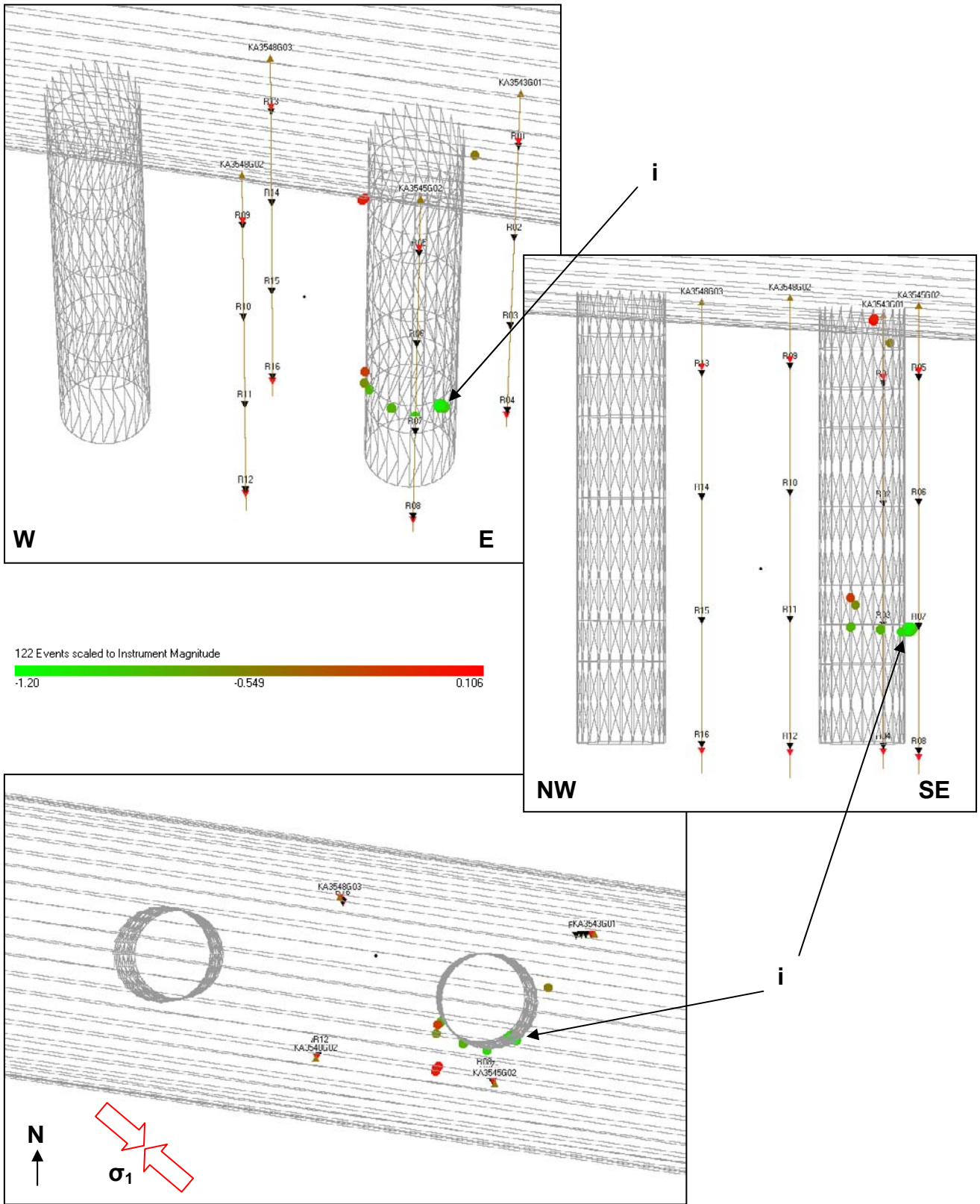


Figure 3-13: Three views of AE activity located around deposition holes DA3545G01 and DA3551G01. (Top: Oblique view looking North; Middle: Transverse view looking north; Bottom: Plan view).

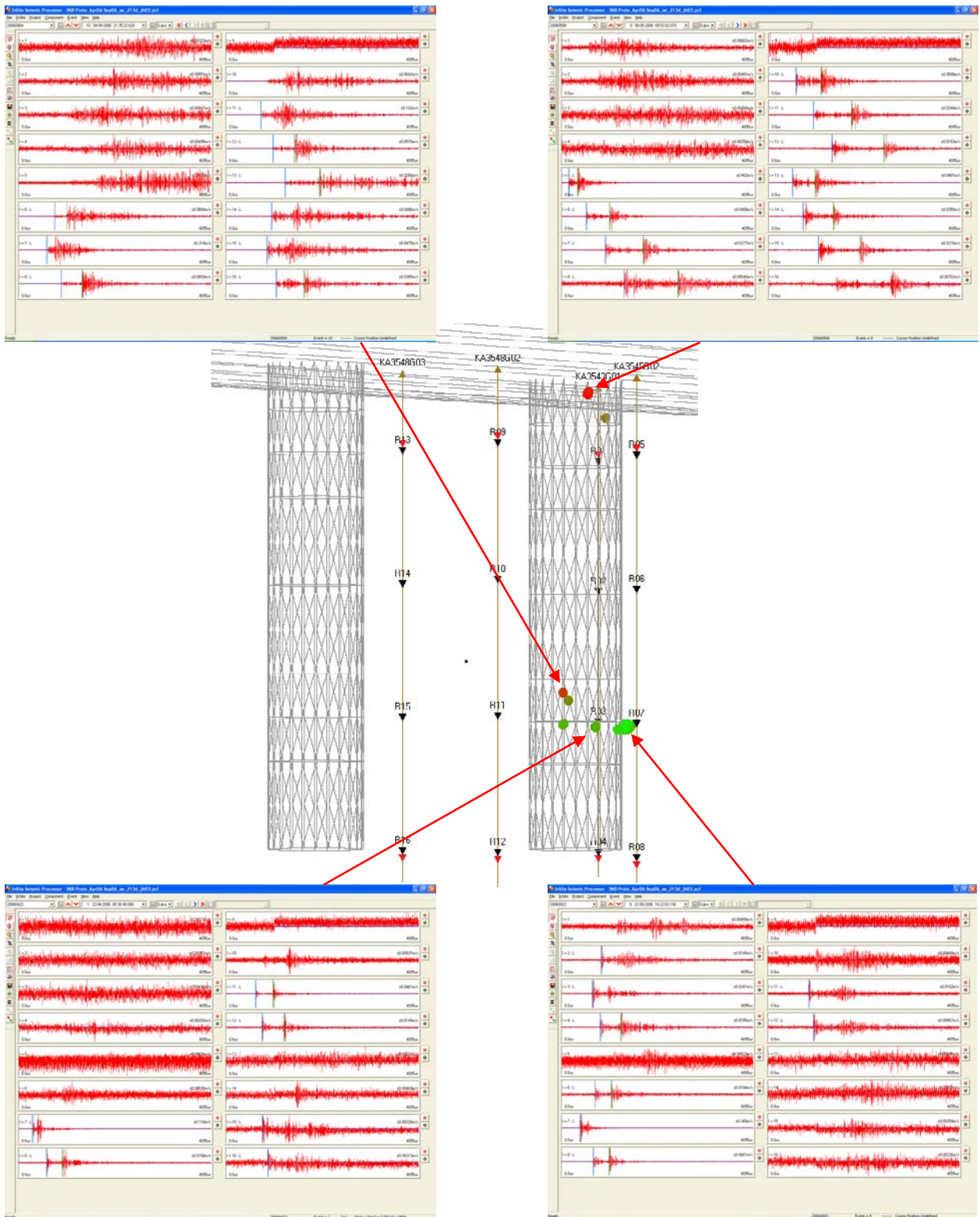


Figure 3-14: Waveforms from selected events shown in relation to a transverse view of AE activity.

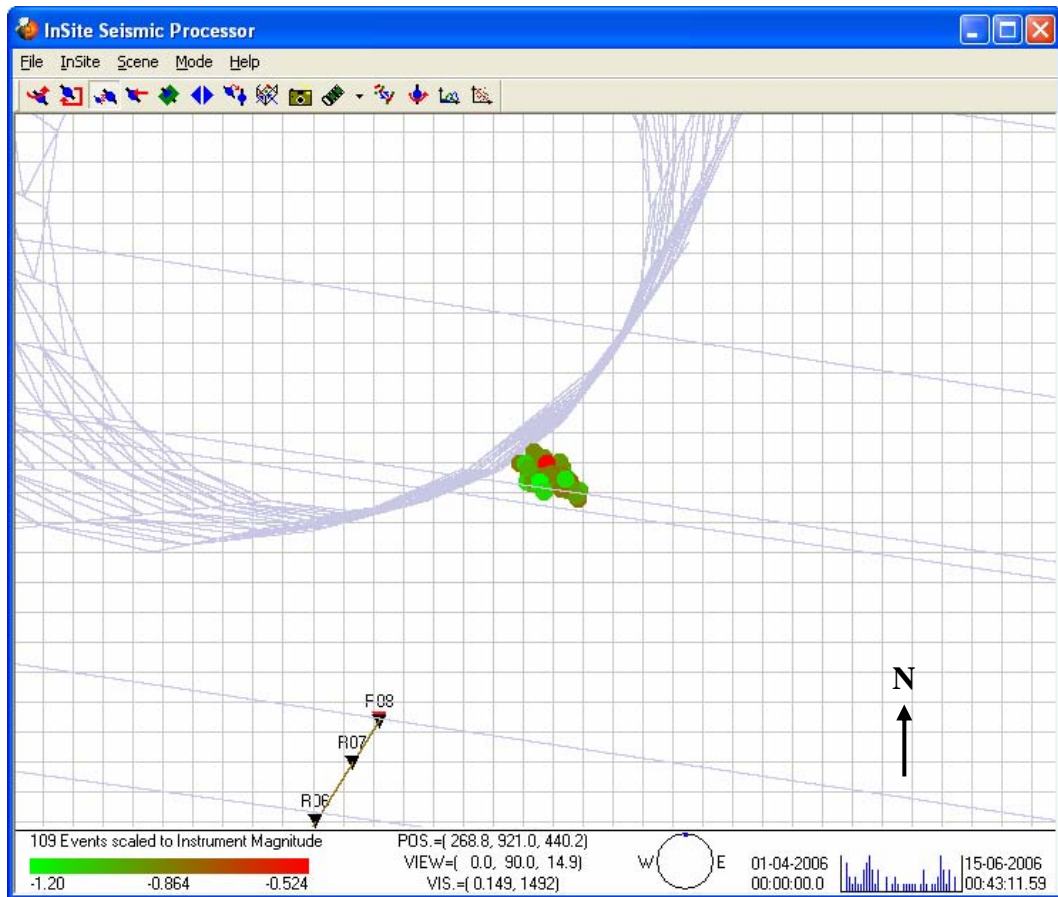


Figure 3-15: Close up plan view of the cluster of 109 events. The background grid is 0.1m in size.

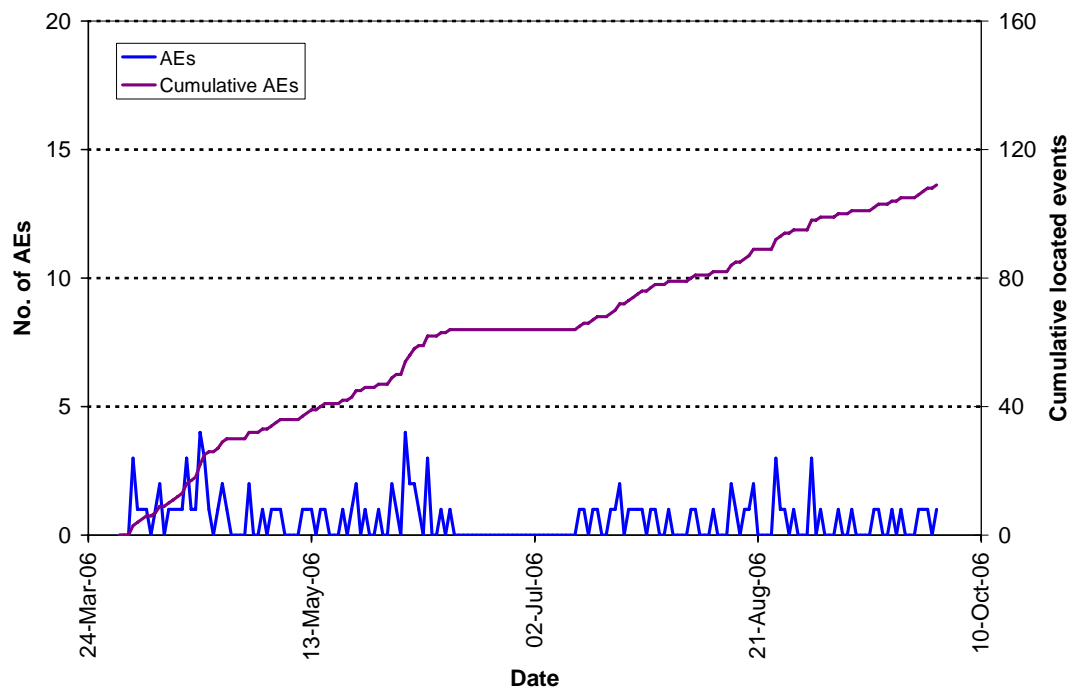


Figure 3-16: Temporal response plot of located AEs in the identified cluster; number per day on left axes and cumulative number right hand axes.

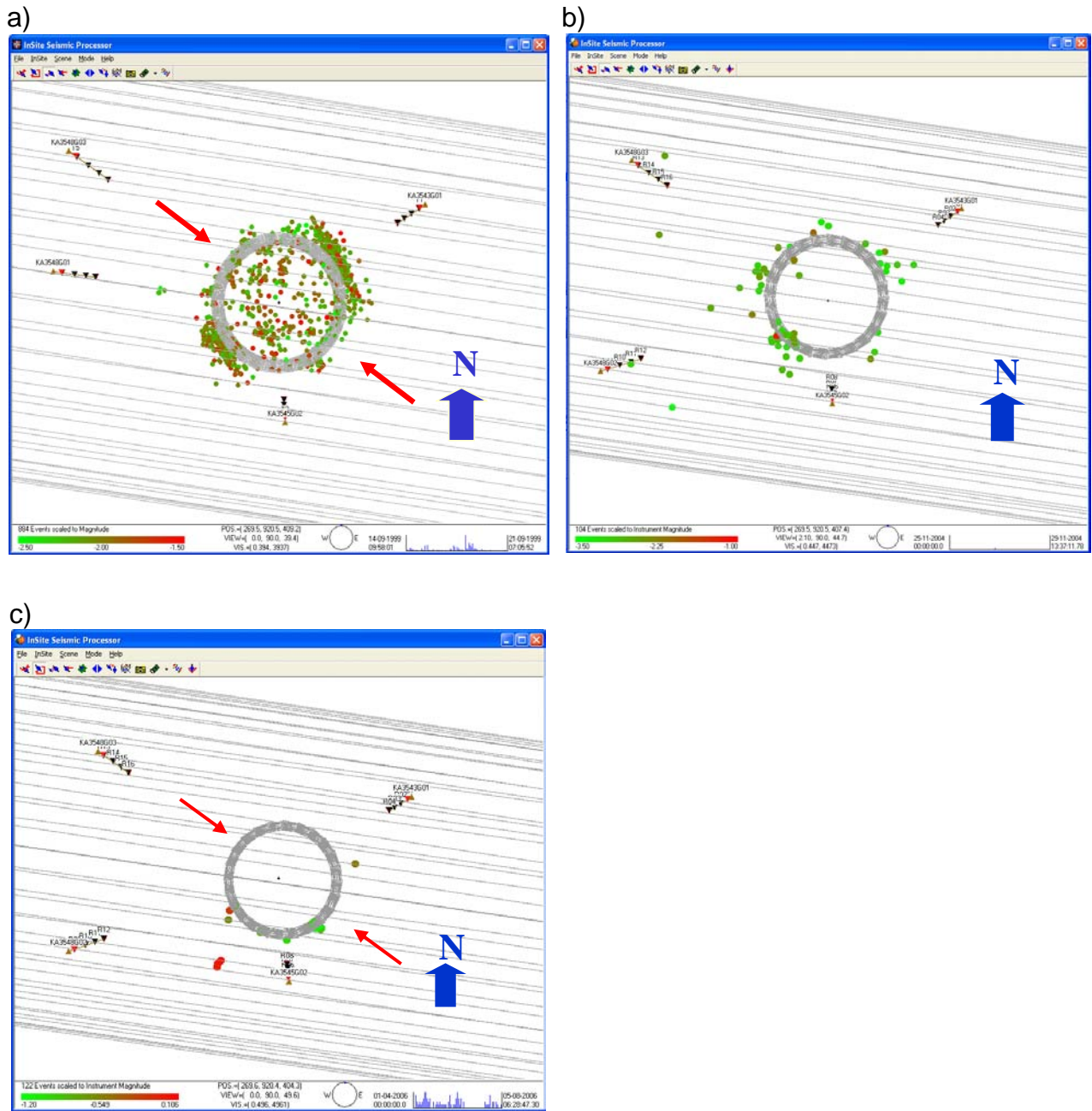


Figure 3-17: Plan view of AEs located around deposition hole DA3545G01 during (a) the excavation phase, (b) the first monitoring phase during heating and (c) this reporting period. The red arrows mark the orientation of the principle stress.

4 Conclusions

4.1 Monitoring Between April and September 2006

- This report describes results from acoustic emission (AE) and ultrasonic monitoring around a canister deposition hole (DA3545G01) in the Prototype Repository Experiment at SKB's Hard Rock Laboratory (HRL), Sweden. The monitoring aims to examine changes in the rock mass caused by an experimental repository environment, in particular due to thermal stresses induced from canister heating and pore pressures induced from tunnel sealing. Monitoring of this volume has previously been performed during excavation [*Pettitt et al.*, 1999], and during stages of canister heating and tunnel pressurisation [*Haycox et al.*, 2005a,b; *Haycox et al.*, 2006]. This report relates to the period between 1st April 2006 and 30th September 2006, and is the third of an ongoing 6-monthly processing and interpretation of the results for the experiment.
- The ultrasonic velocity for each ray path is calculated initially on a 'reference survey' with an estimated uncertainty of $\pm 30\text{m.s}^{-1}$ (± 3 data points). Velocity changes are measured between transmitter-receiver pairs on the daily ultrasonic surveys using a cross-correlation technique that allows a velocity resolution of $\pm 2\text{m.s}^{-1}$. The main reason for the reduction of uncertainty when using the cross-correlation procedure is the dependency of manual picking on the user's judgement of the point of arrival. The cross-correlation procedure then allows for a high-resolution analysis to be performed and hence small changes in velocity to be observed.
- Very little change in P- or S-wave velocity is measured during this monitoring period. The overall trend is for the average P- and S-wave velocity measured between all transmitter-receiver pairs to increase such that velocity is 1.25m.s^{-1} faster for P-wave and 0.70m.s^{-1} faster for S-wave, than at the start. Some larger velocity changes are observed through localised volumes on individual ray paths. P- and S-wave amplitudes decrease initially in the first month (reaching a minimum of 0.11dB), then gradually increase over the remaining time (ending 0.14dB higher than at the start for P-wave amplitude and 0.18dB higher than at the start for S-wave amplitude). The changes in amplitude are less than were recorded during the previous six month reporting period, when both P- and S-wave amplitude decreased, and then increased by over 0.5dB.
- A sudden increase in velocity occurs between 31st August and 1st September. P-wave velocity increases by 1.18m.s^{-1} and S-wave velocity increases by 0.40m.s^{-1} . This is a large change for one day, given that the average is determined from velocity measured on many raypaths. As in previous observations of similar velocity changes, not all ray paths are affected in an identical manner, nor are ray paths purely from one instrumentation borehole to another affected. The change has been interpreted as a localised change in the general rock properties rather than a systematic change in the measurement devices used in the project.

- Changes in Young's Modulus, Poisson's Ratio, Crack Density and Saturation Parameters have been calculated from the average measured velocities for different raypath categories. Saturation is observed to increase to a greater extent on category 'S3'. These raypaths pass through the region of low compressive or tensile stress, and through a possible region of tensile fracturing. This increase may be a result of the slow increase in pressure that could be pressurising fluid into the cracks from the deposition hole. Overall during this six month period, the velocity and amplitude results have shown that the rock mass around the deposition hole has not altered significantly. Gradual increases in temperature and pressure have led to a slow stiffening of the rock, alongside a similarly slow reduction in crack density. During a relatively stable period of environmental characteristics, no dramatic changes in the rock mass have been measured.
- For this reporting period, 122 acoustic emissions have been located with high confidence from 151 triggered events. Activity peaks, in which 4 triggers are recorded on one day, are observed twice on the 18th April and 3rd June. The cumulative plot shows that the rate of triggers remains reasonably constant, however the number of triggers is high in April (1.33 triggers per day), and at the start of June (1.39 triggers per day). On average, 0.98 triggers were recorded per day. An average of 0.80 events are located per day, an increase from the previous 18 months.
- When the spatial distribution of AEs is studied, 109 of the 122 located events are observed to locate in a very tight cluster at a depth of between 455.1 and 455.2m on the south-east of deposition hole DA3545G01. 38 events located in this position during the previous six month reporting period, representing 78% of events located in that period. The cluster locates in a region of low-compressive or tensile stresses. The events are close enough together to be considered as occurring on the same feature and occur over the whole reporting period with no significant peaks in activity. AEs may be occurring at this position due to the presence of a pre-existing microcrack, generated during excavation. Alternatively, the events may result from movement of an instrument positioned on the deposition hole wall. This cluster should be the focus of further investigation.
- For the past year, a greater proportion of events have been locating in the low-compressive regions in the NW and SE quadrants. Before this, during excavation and initial heating, the majority of the events located in the NE and SW quadrants. These regions are subject to increased compressive stresses, as identified from the insitu stress field by *Pettitt et al.*[1999]. Smaller clusters were observed in the orthogonal regions of low-compressive or tensile stress. It is important to note that events located during this reporting period are consistent with previous results, i.e. no events are positioned in regions where activity has not been observed in the past. The events can therefore be interpreted as a continuation of activity in the damage zone, and could be created either by movement on pre-existing microcracks, or as a result of extension or formation of new microcracks in the existing damaged region. The numbers of events are relatively low and therefore indicate the rock mass around the deposition holes has remained stable during this six-month period.

4.2 Summary of Monitoring from the Heating and Pressurisation Phase

- Monitoring of the heating and pressurisation phase at the Prototype Repository Experiment has been conducted since March 2003. *Haycox et al.*[2006] present a detailed analysis of the ultrasonic measurements obtained in this phase to the end of March 2006, and split the experiment into four periods for analysis based on environmental factors (Figure 4-1). Monitoring of the past six months has shown the rock response to be a continuation of the fourth period starting November 2005 consistent with temperature and pressure measurements from other instruments during this reporting period (*Gourdazi*[2006]) that show a slow increase, with no sudden or high magnitude changes. Table 4-1 presents a summary of the observations from ultrasonic monitoring thus far, and Table 4-2 provides interpretations of the rock response after *Haycox et al.*[2006].
- Figure 4-1 shows average P- and S-wave velocity and amplitude recorded during the monitoring. Figure 4-2 to Figure 4-6 provides average velocity and modulus changes for the six raypath categories selected in terms of disturbed and damaged regions (Figure 3-5). Figure 4-7 and Figure 4-8 show all locations and the temporal distribution of located AEs recorded since March 2006. Figure 4-9 to Figure 4-12 summarise changes that take place at different regions around the deposition hole in schematic diagrams for each period, identifying the primary changes in the properties of the rock as described in Table 4-2.

4.3 Recommendations

1. Further investigation of the cluster of events on the SE side of deposition hole DA3435G01 should be undertaken. This would include an attempt to determine source mechanisms of the events, which is possible because waveforms are recorded on sensors in three instrumentation boreholes. This analysis would investigate the typical source mechanism occurring in the cluster, and whether this changes over time, with the objective of resolving the primary factors responsible for causing AEs in that particular position.
2. The OMNIBUS Project (*Pettitt et al.*[2004]), part funded by the EC in the 5th EURATOM framework, investigated changes in waveform character from ultrasonic surveys during excavation at the Prototype Repository. The method compared the measured observations with full-waveform modelling of the experiment. This analysis should be extended to the monitoring of changes in temperature and pressure over the past two years with the objective of helping us further understand the physical mechanisms by which the rock has changed its properties.

Table 4-1: Summary of velocity, amplitude and AE variation measured during four periods of temperature and/or pressure change.

Name / Date	Temperature/Pressure	Velocity	Amplitude	AE
PERIOD 1 25 th May 2003 to 31 st October 2004	Heaters in canister switched on causing an initially rapid change in temperature which gradually levels out to a constant increase. An increase of 35°C is measured for an instrument in rock adjacent to the deposition hole. Pressure constant	Rapid increase in P- and S-wave velocity on 'S3' category. Other categories show increases but to a lesser extent. Initial decrease in P-wave velocity in comparison to S-wave velocity for all raypaths except for 'S3'.	Amplitudes increase over this period by between 3dB and 9dB for P-wave amplitude, and 7dB and 12dB for S-wave amplitude.	AEs do not start immediately after heating. This could be a Kaiser-type effect in which AE rate remains close to background level until stress increases above the largest previous value. Peak of 13 events located on 26 th June 2003. Average Event Rate = 0.5 / day
PERIOD 2 1 st November 2004 to 4 th September 2005	Drainage to tunnel closed on 1 st November. Pressure in tunnel increases. Pressure increases measured in the deposition-hole buffer between 3 rd and 5 th December. Damage observed on canister on 6 th December so drainage reopened and heaters switched off. Power switched on 15 th December.	Velocity increases measured close to the tunnel from 26 th November. Larger increases measured on categories 'S1' and 'S3'.	Amplitude increases measured close to the tunnel from 26 th November.	Relatively large number of events recorded in this period. Peak rate of 32 AEs on 4 th and 5 th December. Events locate in clusters in previously observed damage zone. Average Event Rate = 0.4 / day
PERIOD 3 5 th September 2005 to 2 nd November 2005	Additional drainage is opened in August 2005 leading to a decrease in pressure and temperature. Heaters turned off on 5 th September	P- and S-wave velocities decrease on all raypath categories except 'far'.	P-wave amplitude decrease on all category raypaths.	Slight increase in event rate above background rate recorded in previous 5 months. Average Event Rate = 0.3 / day
PERIOD 4 3 rd November 2005 to 30 th September 2006	Pressure in tunnel increases. Constant increase in pressure in buffer above deposition hole. Heaters switched on again so temperature around deposition hole increases.	P- and S-wave velocities increase on all category raypaths. Larger increases measured on 'S3'.	P- and S-wave amplitude increase on the majority of raypaths.	Cluster of 148 events located on SE side of deposition hole. Similar rate of AE locations. Average Event Rate = 0.5 / day

Table 4-2: Summary of key interpretation of rock response from the ultrasonic measurements.

Period	Summary of Key Interpretations
1	<p>The heaters are switched on. The 'S3' category passes through a volume that is unloaded and hence experiences low compressive stresses. This volume responds more rapidly to thermal stresses because existing microfractures are initially unloaded and hence more open than microfractures in the compressive region. P- and S-wave velocities decrease a similar amount during excavation as they increase during heating. This suggests very strongly that the microfractures induced in the regions of tensile damage around the deposition hole close when thermal stresses are applied. The difference in the rate of response between raypaths in the compressive categories was interpreted as a different magnitude of response of the microfractures in the rock mass to increasing thermal stresses.</p> <p>In the first few months of heating, another effect is superimposed onto the rock's response to thermal stresses. This is measured as a reduction in P-wave velocities compared to S-wave velocities in the first few months of heating. This is particularly noticeable on 'S1' category in Figure 4-2, in which P-wave velocity decreases by about $3.5\text{m}\cdot\text{s}^{-1}$ while S-wave velocity remains constant. A desaturation occurs on all raypath categories, other than 'S3'. This must be caused by a drying of the rock mass, in the zones experiencing high compressive stresses, as heat is applied to the rock (i.e. both temperature and pressure are acting to expel moisture). In the low-compressed, or tensile, region saturation increases during this period. This is probably caused by hot fluids expanding into the open microfracture fabric.</p>
2	<p>Pressure rose rapidly after drainage from the tunnel was closed. This resulted in damage to the canister and the heaters being temporarily switched off. Temperature around the deposition hole reduced rapidly, but started increasing again after 13 days. Significant changes to the character of many recorded ultrasonic waveforms were observed as significant increases in signal quality. This suggests that as pressure increased in the rock surrounding the deposition hole, attenuation of the ultrasonic waves is significantly reduced meaning that they can pass more efficiently through the rock medium.</p> <p>The pressure increase can be interpreted as increasing the stiffness of the rock with a corresponding decrease in crack density. The magnitude of increase is greater for 'S1' and 'S3' categories because the volumes through which they pass are close to the deposition holes and contain a higher proportion of microfractures in an excavation damage zone. The pressure increase acts as a confining pressure on the rock mass leading to a closure of the pre-existing microcrack fabric and so a reduction in crack density. We observe that only a relatively small pressure increase is sufficient to close this microcrack fabric in the volumes already under high compressive stresses, leading to an initially high rate of change in measured velocities followed by a constant level, even though pressures may keep increasing afterwards. From Figure 4-2 the required pressure increase is approximately 1.5MPa.</p> <p>The rapid pressure increase led to 32 events locating in clusters over the course of two days. The events are interpreted as stress changes in the rock as it responds to the sudden pressure change. This induces small scale movement on pre-existing microcracks, or induces new microfractures in weaker volumes of the rock. Pore pressure increases may also have assisted in inducing slip on pre-existing microfractures, by reducing the normal stress on the fractures. Over the rest of this period, as pressure continued to increase, fewer events were located.</p> <p>Another effect at this time is a rapid cooling of the rock when the heater inside the canister is switched off (for 13 days between 2nd and 15th December 2004), followed by warming as the rock is reheated. The majority of categories do not show a significant change in P- or S-wave velocity during this period indicating they are relatively insensitive to temperature changes at this time (i.e. when pressures are high). The exception is category 'S3', which exhibits a decrease in P- and S-wave velocity followed by an increase that mirrors the rate at which temperature changes (Figure 4-3). This category was found to be the most sensitive to thermal stresses during the initial stages of heating. When the rock cools, thermal stresses acting in this volume of low compressive (or slightly tensile) stresses reduce causing unloading of the microcracks. Microcracks close again when the rock is reheated and thermal stresses increase.</p>

3	<p>In September 2005 additional drainage from a permeable mat placed on the inner surface of the outer plug was opened, and heaters were switched off. This resulted in a cooling and de-pressurisation of the deposition hole. Neither temperature nor pressure reduced to the background level.</p> <p>The decrease in velocity on most raypaths is generally low compared to the increases observed previously. An exception to this is category 'S3'. This category is observed as the most sensitive. As temperature and pressure decreases, stresses again reduce in this volume causing microcracks to reopen and resulting in an increase in crack density and reduced stiffness of the rock.</p> <p>At the start of the period a sudden (over a few days), but relatively small change in velocity is observed, superimposed on the longer-term trends. We believe these are related to rapid changes in fluid pressure; a corresponding increase is observed at the end of the period (start of Period 4). For Period 3, an increase in Young's Modulus occurs which indicates a stiffening of the rock. This short term change is therefore likely to be a sudden reaction of the rock mass to the decrease in fluid pressure, perhaps caused by a general closing of microcracks caused by decreased pore pressures. The reverse is true for Period 4, when a pressure increase leads to a general opening of microcracks caused by increased pore pressures. This is believed to be a different response to long term trends from thermal stresses and general confining of the rock mass.</p>
4	<p>During the fourth period, heaters were turned back on once more causing temperature around the deposition hole to increase. Pressure increased rapidly again, probably caused by changes in the buffer temperature (changes in water volume caused by the temperature in combination with low hydraulic conductivity) [Johannesson, 2006]. Velocity increases rapidly at first, then at a constant rate, following a similar pattern to the temperature and pressure.</p> <p>Raypath category 'S3' exhibits the greatest increase in P and S-wave velocity. Similar patterns are observed on 'S1' and 'C1', and to a lesser extent on 'C2'. Velocity on the 'far' raypath category remains constant throughout the period. When temperature and pressure start to increase the stiffness of the rock increases, particularly on 'S3'. This is accompanied by a reduction in crack density. The associated increase in stiffness and decrease in crack density can be interpreted as the closing of existing microfractures and pore spaces as observed previously. This effect has continued to the current day.</p> <p>Few events have been located during Periods 3 and 4. A rapid decrease, and then increase, in pressure and temperature appears to have no significant affect on the number, or distribution of AEs around the deposition hole. The AE rate marginally increased since February 2006 (Figure 4-8). The vast majority of events locate on a single cluster in the south-east of the deposition hole and at 455.1m depth. The low number of AEs suggests the rock mass has stabilised. The high pressures result in a confining pressure being placed on the rock around the deposition hole and inhibit the movement on microcracks or macrofractures.</p>

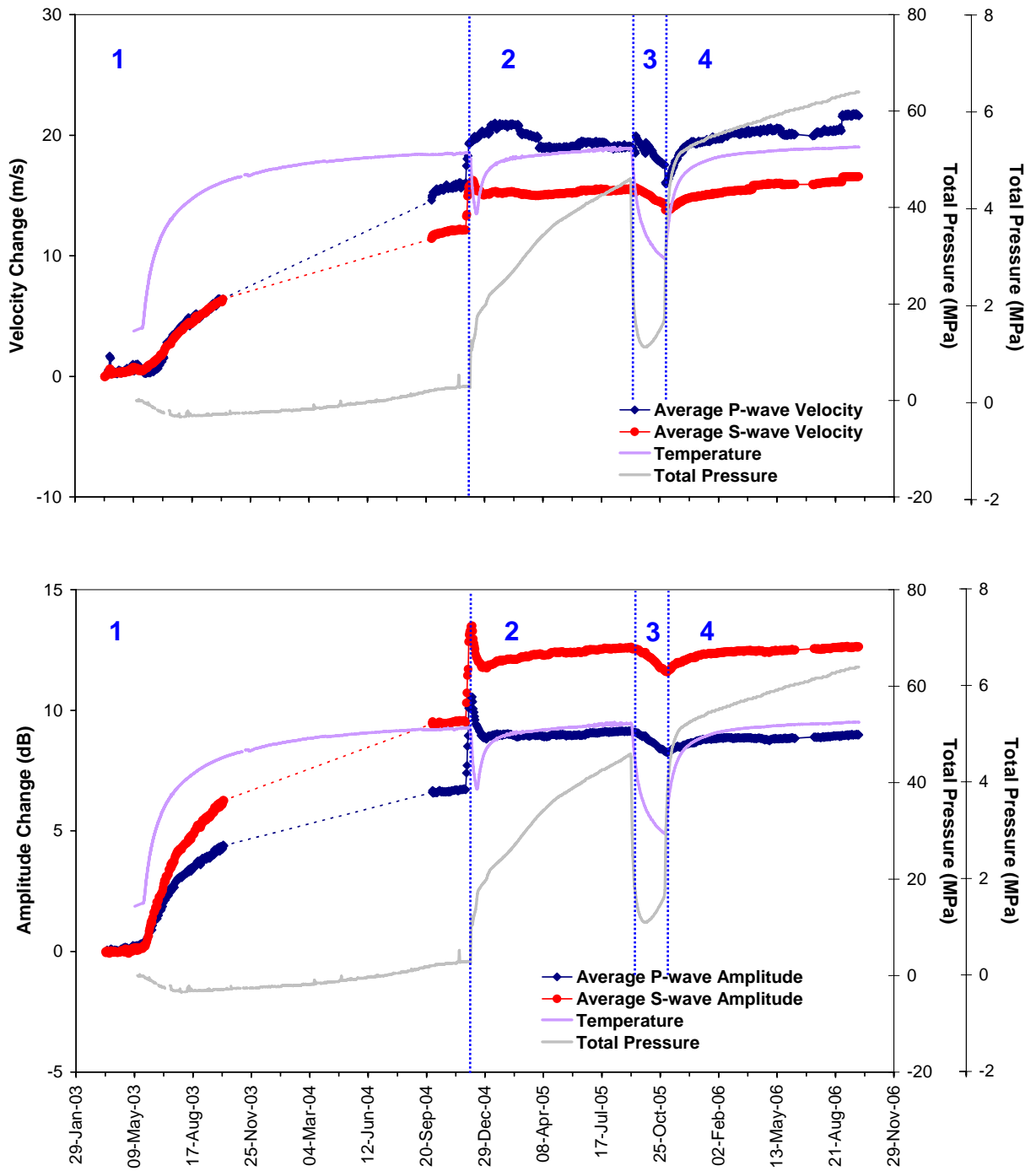


Figure 4-1: P- and S-wave (a) velocity change and (b) amplitude change from the start of monitoring, plotted alongside temperature (TR6045) and pressure (PB616) measurements in deposition hole DA3545G01. The vertical blue lines differentiate between periods of similar environmental conditions (see Table 4-1).

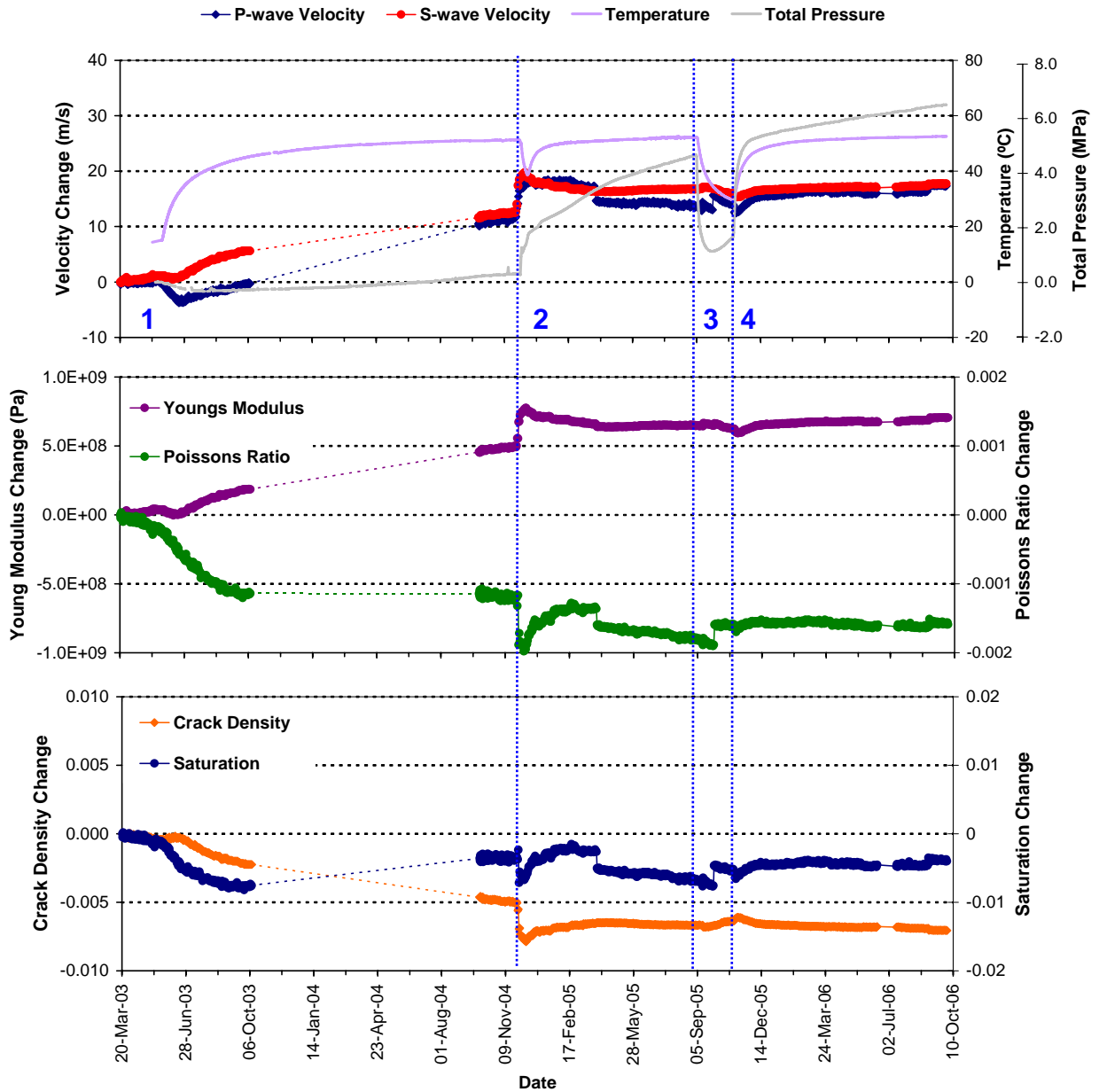


Figure 4-2: Average P- and S-wave velocity change for raypaths on category 'S1' together with temperature (TR6045) and total pressure (PB616) (top), Young's Modulus and Poisson's Ratio change (middle), and Crack Density and Saturation change (bottom).

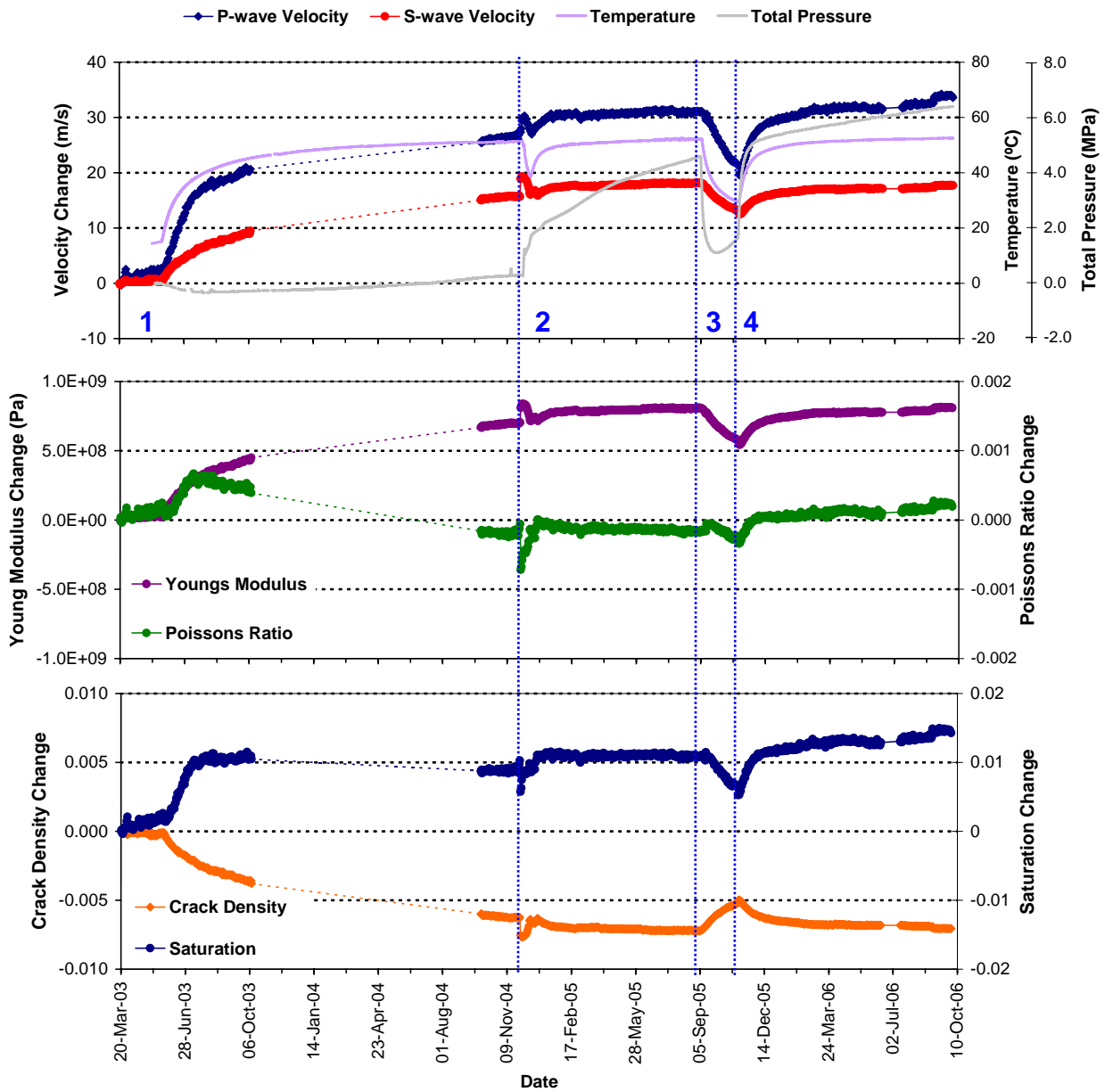


Figure 4-3: Average P- and S-wave velocity change for raypaths on category 'S3' together with temperature (TR6045) and total pressure (PB616) (top), Young's Modulus and Poison's Ratio change (middle), and Crack Density and Saturation change (bottom).

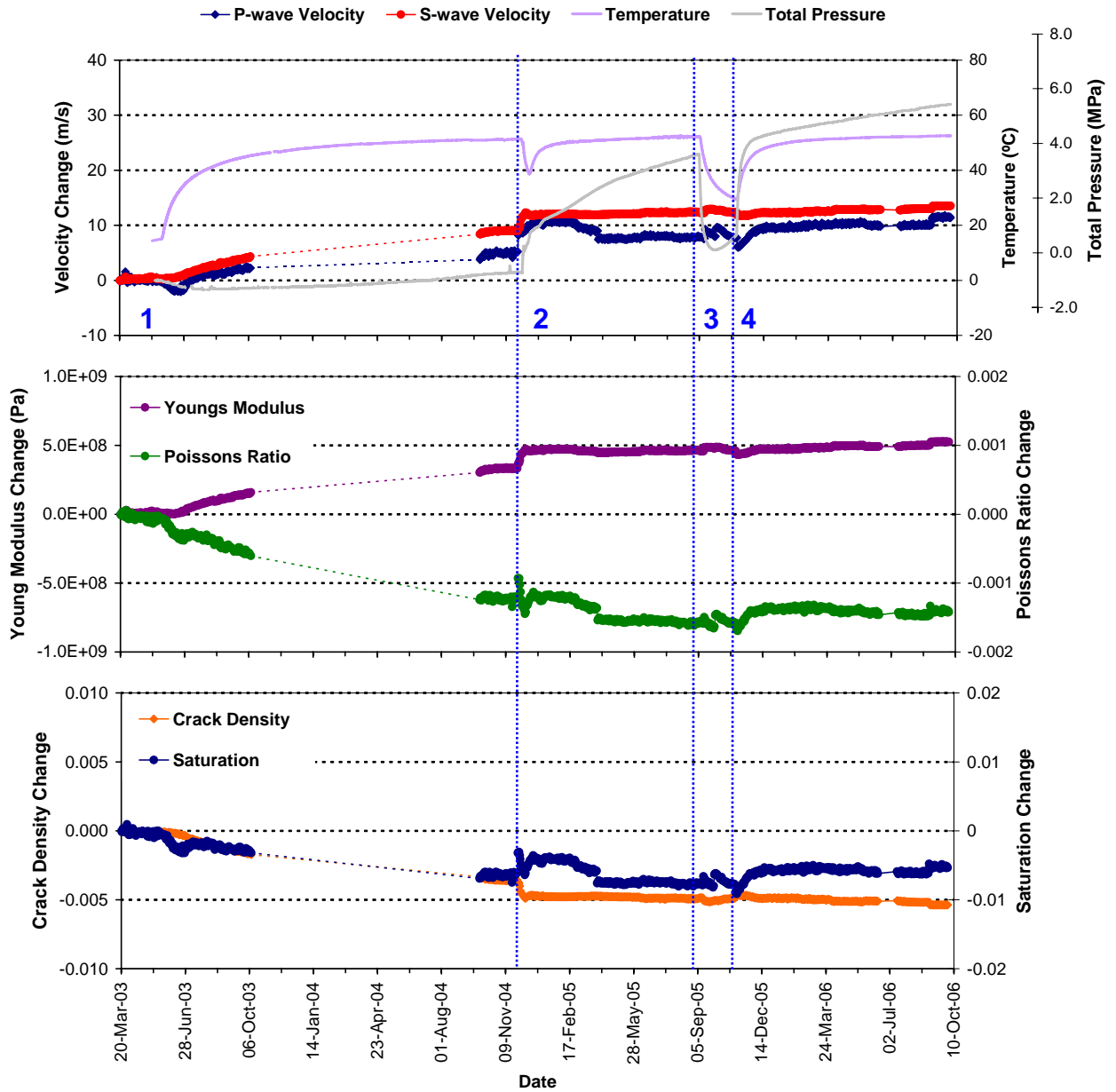


Figure 4-4: Average P- and S-wave velocity change for raypaths on category 'C1' together with temperature (TR6045) and total pressure (PB616) (top), Young's Modulus and Poisson's Ratio change (middle), and Crack Density and Saturation change (bottom).

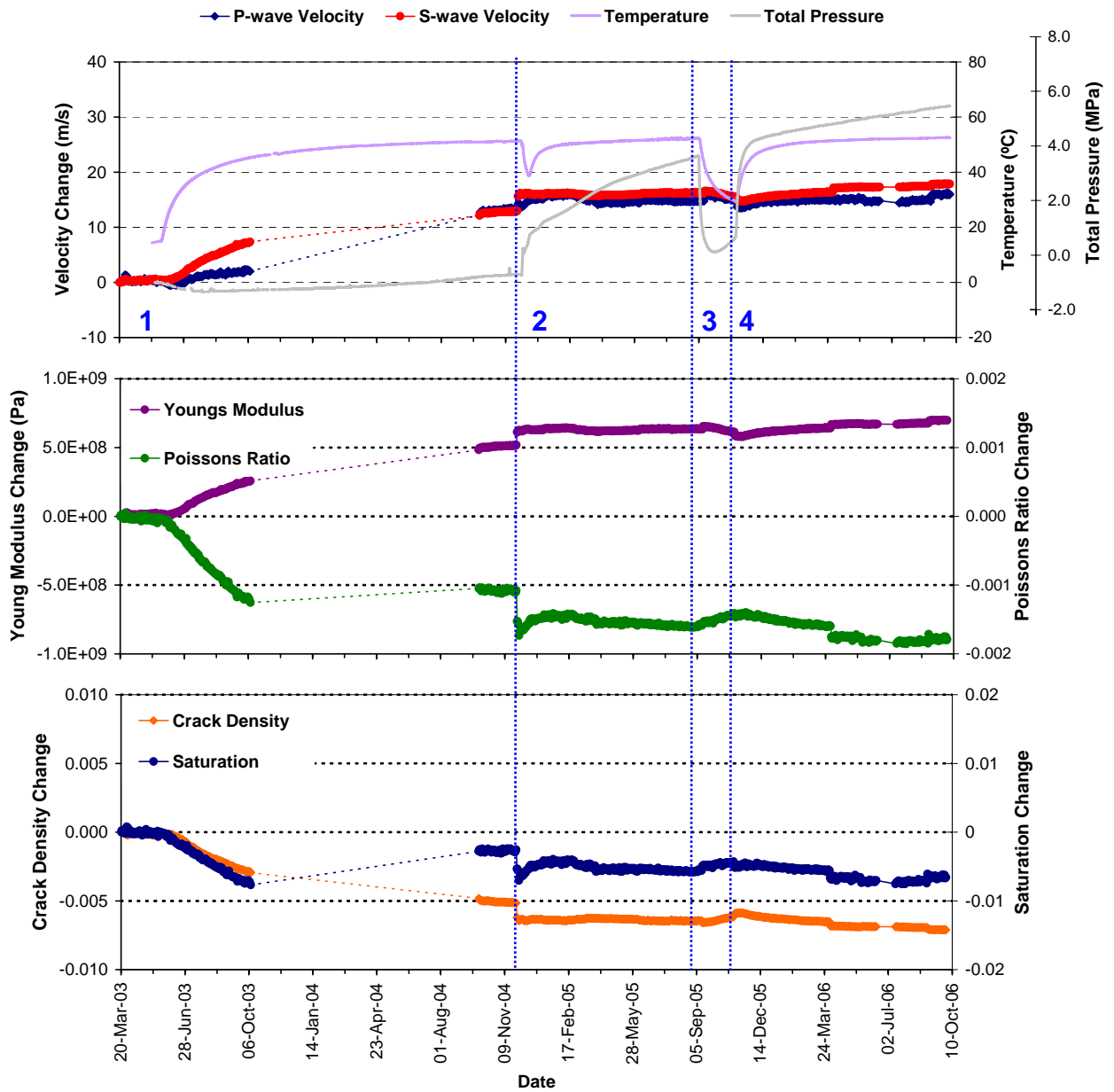


Figure 4-5: Average P- and S-wave velocity change for raypaths on category 'C2' together with temperature (TR6045) and total pressure (PB616) (top), Young's Modulus and Poisson's Ratio change (middle), and Crack Density and Saturation change (bottom).

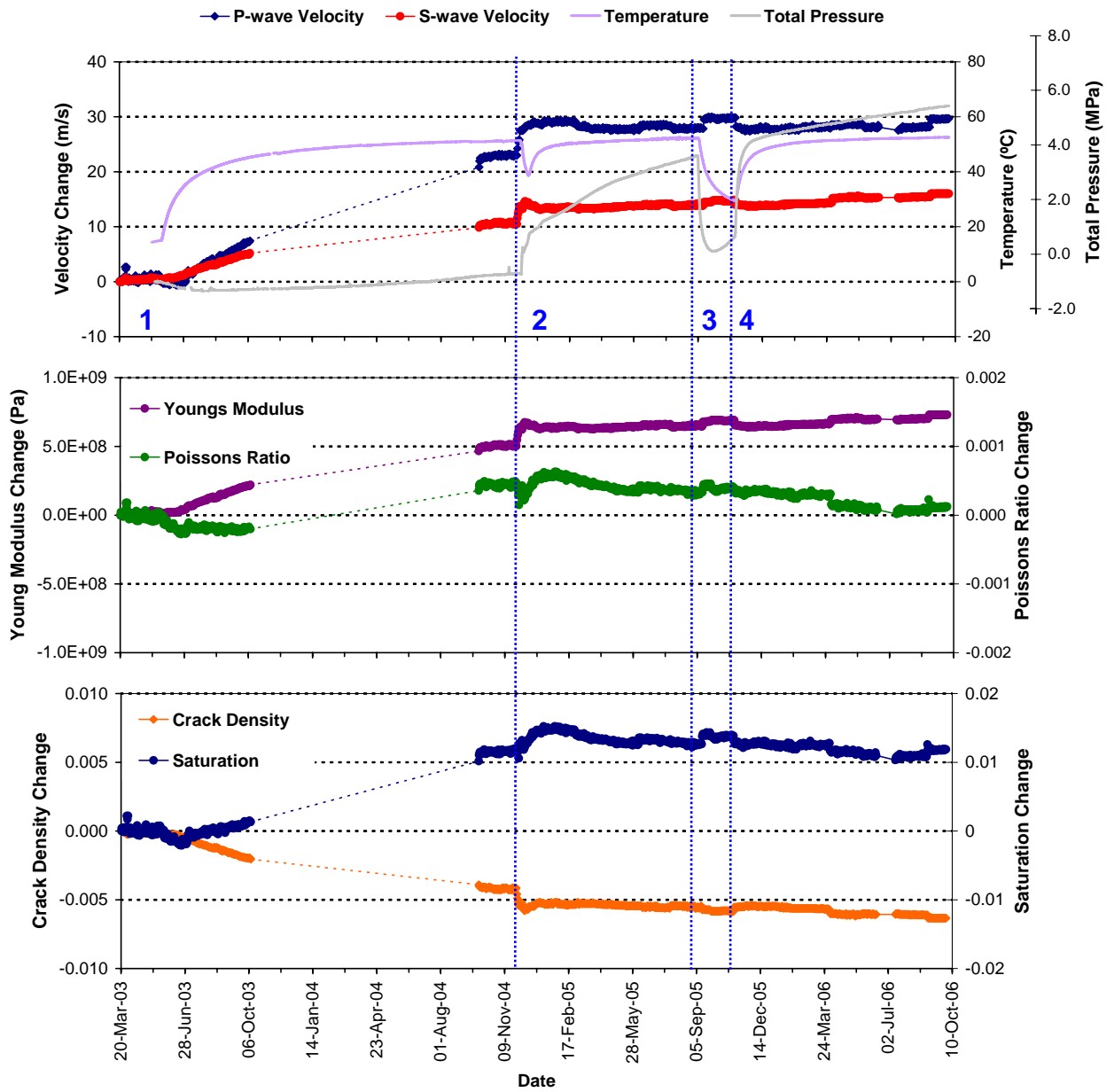


Figure 4-6: Average P- and S-wave velocity change for raypaths on category 'Far' together with temperature (TR6045) and total pressure (PB616) (top), Young's Modulus and Poisson's Ratio change (middle), and Crack Density and Saturation change (bottom).

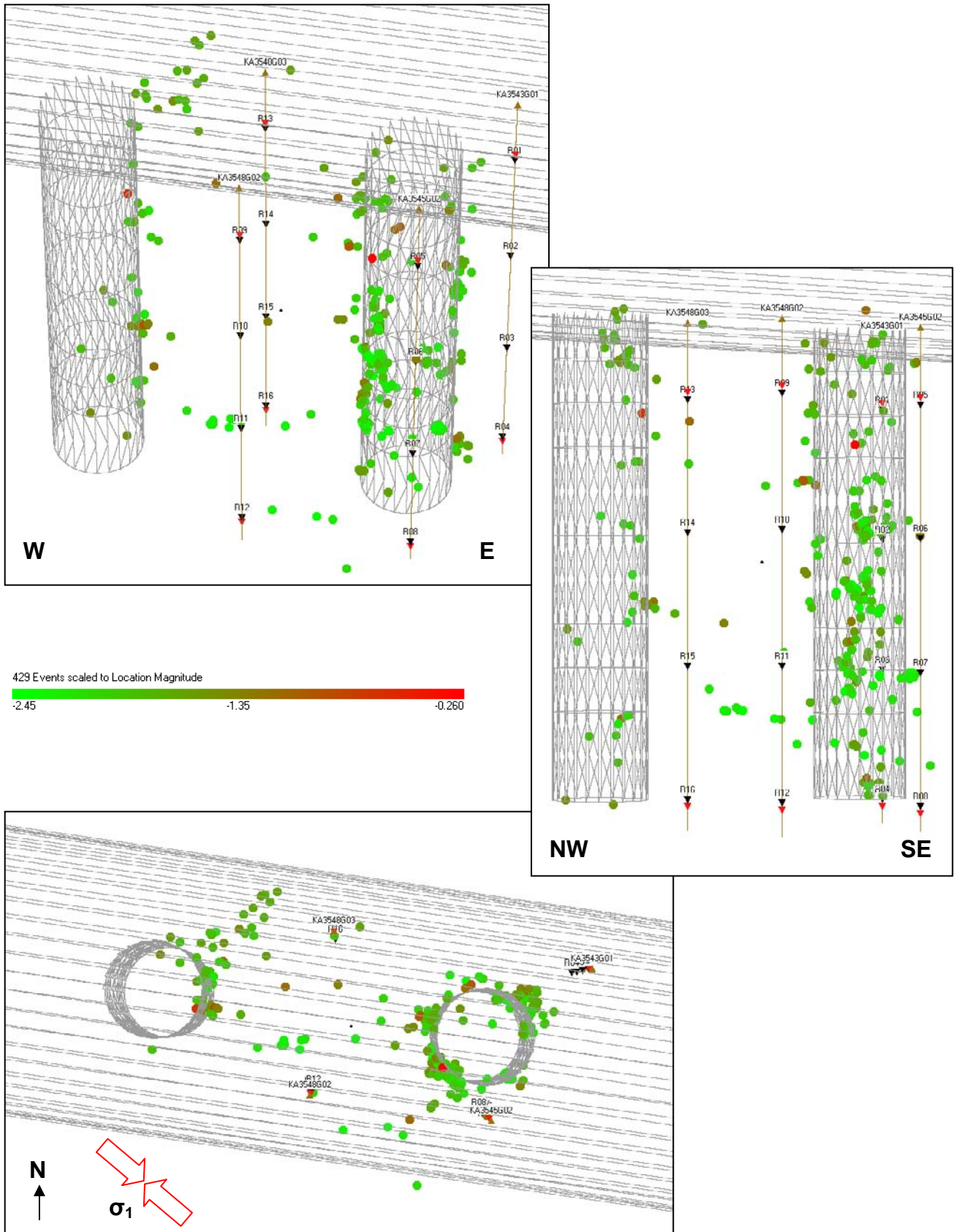


Figure 4-7: Projections of all AEs located during the heating phase. Events are scaled to location magnitude.

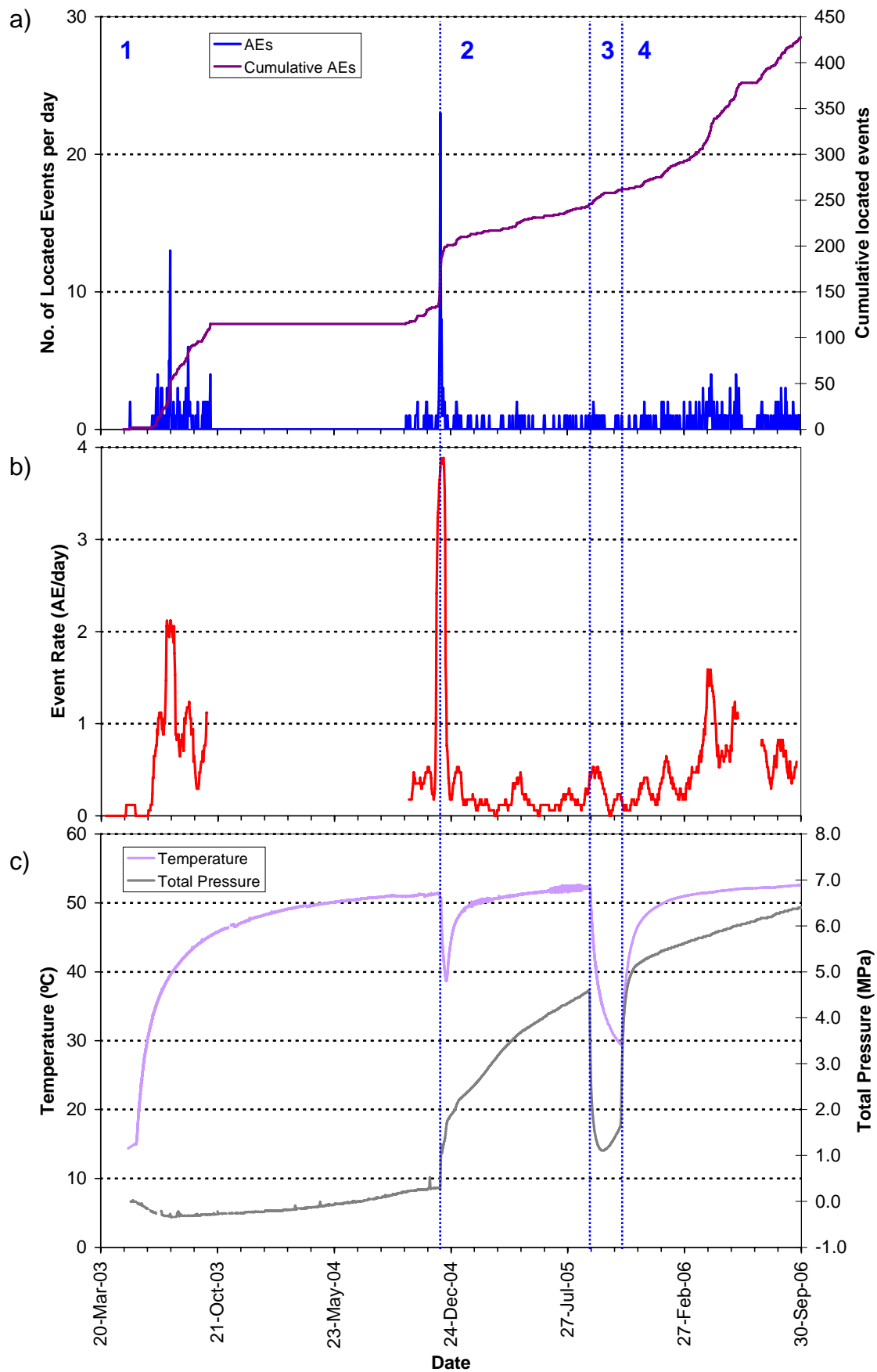


Figure 4-8: (a) Number and cumulative number of located events from the start of monitoring, (b) average number of AE events per day (averaged over 17 days) and (c) temperature (TR6045) and pressure (PB616) measurements in deposition hole DA3545G01.

PERIOD 1
25th May 2003 to
31st October 2004

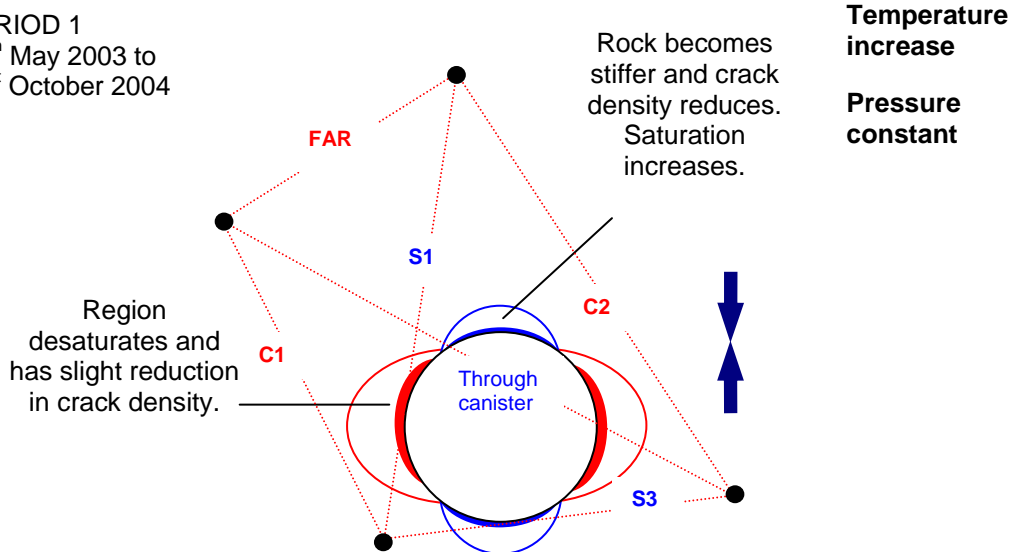


Figure 4-9: Schematic diagram of the deposition hole and explanation of changes experienced during Period 1.

PERIOD 2
1st November 2004 to
4th September 2004

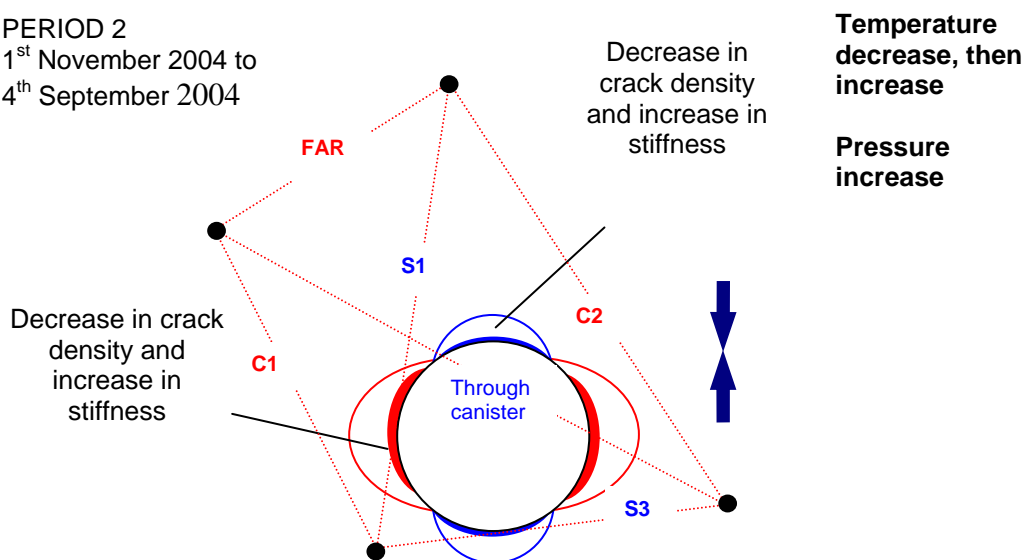


Figure 4-10: Schematic diagram of the deposition hole and explanation of changes experienced during Period 2.

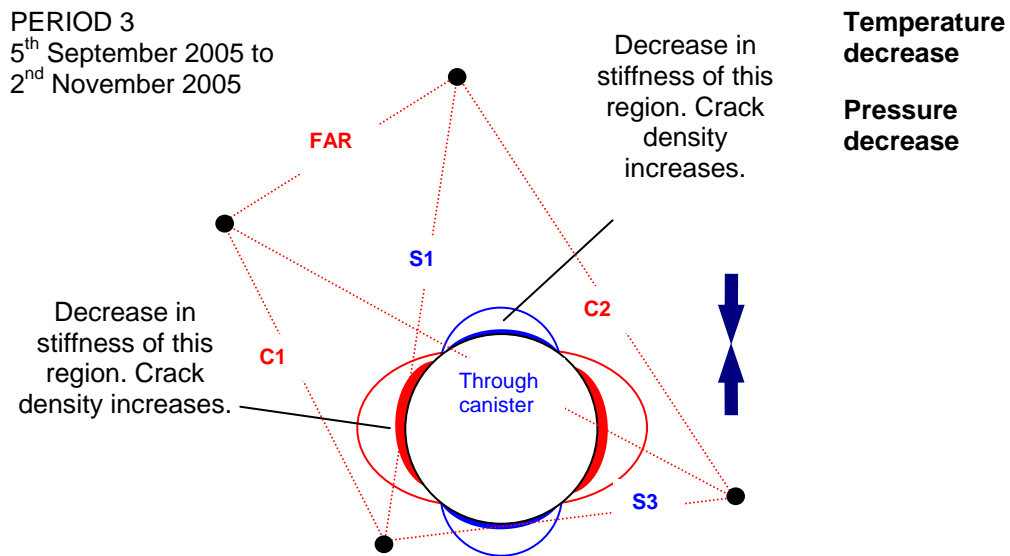


Figure 4-11: Schematic diagram of the deposition hole and explanation of changes experienced during Period 3.

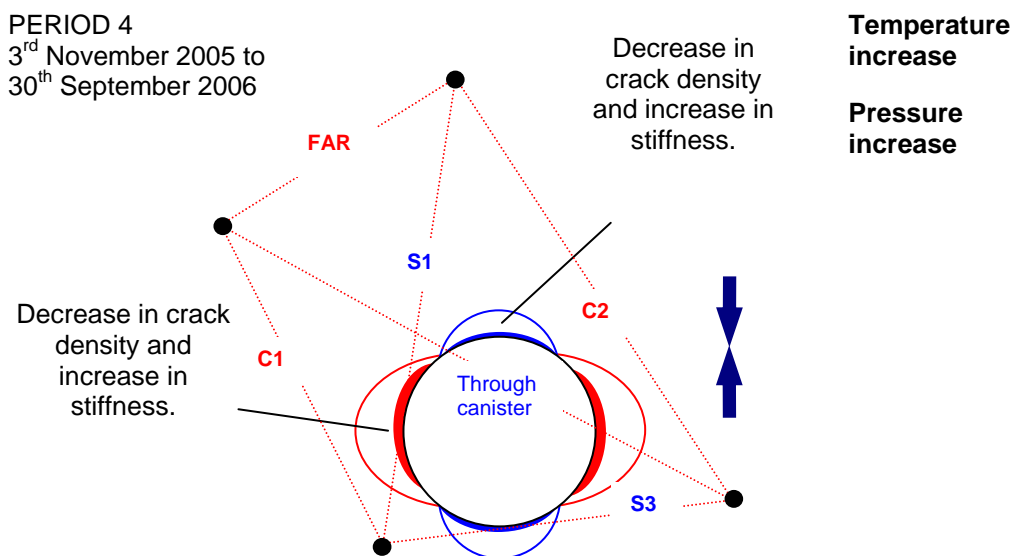


Figure 4-12: Schematic diagram of the deposition hole and explanation of changes experienced during Period 4.

References

Baker, C. and R.P. Young. 2002. Acoustic emission and ultrasonic monitoring around the TSX tunnel clay and concrete bulkheads between October 2001 and October 2002. Ontario Power Generation, Nuclear Waste Management Division Report.

Goudarzi, R. and L-E. Johannesson, Sensor Data Report (Period: 010917-050601). Prototype Repository. Report No: 13, International Progress Report IPR-05-28, Äspö Hard Rock Laboratory, Swedish Nuclear Fuel and Waste Management Company, Sweden, 2006.

Goudarzi, R., 2006. Pers. Comm.

Haycox, J.R., W.S. Pettitt, and R.P. Young, Acoustic Emission and Ultrasonic Monitoring During the Heating of Deposition hole DA3545G01 in the Prototype Repository to March 2005, International Progress Report IPR-05-30, Äspö Hard Rock Laboratory, Swedish Nuclear Fuel and Waste Management Company, Sweden, 2005a.

Haycox, J.R., W.S. Pettitt, and R.P. Young, Acoustic Emission and Ultrasonic Monitoring Results from Deposition Hole DA3545G01 in the Prototype Repository between April 2005 and September 2005, International Progress Report IPR-05-31, Äspö Hard Rock Laboratory, Swedish Nuclear Fuel and Waste Management Company, Sweden, 2005b.

Haycox, J.R., W.S. Pettitt, and R.P. Young, Acoustic Emission and Ultrasonic Monitoring Results from Deposition Hole DA3545G01 in the Prototype Repository between October 2005 and March 2006, Report for Swedish Nuclear Fuel and Waste Management Company, Sweden, 2006.

Maxwell, S.C., and R.P. Young, A controlled in-situ investigation of the relationship between stress, velocity and induced seismicity, *Geophys. Res. Lett.*, 22, 1049-1052, 1995.

Patel, S., L.-O. Dahlstrom, and L. Stenberg, Characterisation of the Rock Mass in the Prototype Repository at Äspö HRL Stage 1, Äspö Hard Rock Laboratory Progress Report HRL-97-24, Swedish Nuclear Fuel and Waste Management Company, Sweden, 1997.

Pettitt, W.S., C. Baker, and R.P. Young, Acoustic emission and ultrasonic monitoring during the excavation of deposition holes in the Prototype Repository, International Progress Report IPR-01-01, Äspö Hard Rock Laboratory, Swedish Nuclear Fuel and Waste Management Company, Sweden, 1999.

Pettitt, W.S., C. Baker, and R.P. Young, Analysis of the in-situ principal stress field at the HRL using acoustic emission data, International Progress Report IPR-01-09, Äspö Hard Rock Laboratory, Swedish Nuclear Fuel and Waste Management Company, Sweden, 2000.

Pettitt, W.S., C. Baker, R.P. Young, L. Dahlstrom, and G. Ramqvist, The assessment of Damage Around Critical Engineering Structures Using Induced Seismicity and Ultrasonic Techniques, *Pure and Applied Geophysics*, 159, 179-195, 2002.

Pettitt, W.S., D.S. Collins, M.W. Hildyard, R.P. Young, C. Balland and P. Bigarré. 2004. An Ultrasonic Tool for Examining the Excavation Damaged Zone around Radioactive Waste Repositories – The OMNIBUS project, in *EC Euradwaste04 Conference*, Luxembourg.

Pettitt, W.S., Baker, C., Collins, D.S., and R.P. Young, 2005. InSite Seismic Processor – User Operations Manual Version 2.13. Applied Seismology Consultants Ltd., Shrewsbury, UK.

SKB, Äspö Hard Rock Laboratory: Current Research Projects 1998. Swedish Nuclear Fuel and Waste Management Company, Sweden, 1999.

Telford, W.M., Geldart, L.P., and Sheriff, R.E., *Applied Geophysics: Second Edition*, Cambridge University Press, 1990.

Young, R.P. and W.S. Pettitt, Investigating the stability of engineered structures using acoustic validation of numerical models, in *Geotechnical Special Publication No 102*, edited by J.F. Labuz, S.D. Glaser, and E. Dawson, pp. 1-15, ASCE, USA, 2000.

Zimmerman, R.W and M.S. King, Propagation of acoustic waves through cracked rock, 20th Symposium on Rock Mechanics, Rapid City, SD, 1985.

Appendix I Previous Monitoring at the Prototype Repository

Ultrasonic monitoring has been conducted at the Prototype Repository in some form since September 1999. During excavation, monitoring of both deposition holes in Tunnel Section 2 (DA3551G01 and DA3545G01) was undertaken to delineate zones of stress related fracturing and quantitatively measure fracturing in the damaged zone [Pettitt *et al.*, 1999]. Thereafter, monitoring has been undertaken on a single deposition hole (DA3545G01), and the response of the surrounding rock to changes in temperature and pressure has been measured (see Haycox *et al.*[2005a] and Haycox *et al.*[2005b]). The previous report, by Haycox *et al.*[2006], was the first of an ongoing 6-monthly processing and interpretation of the results. This report presents new results from the period 1st March 2006 to 30th September 2006. Further details of the ultrasonic monitoring are shown in Table 4-3 and described below.

Table 4-3: Summary of ultrasonic monitoring at the Prototype Repository to-date. Response Periods are defined in Haycox *et al.*[2006].

Report	Monitoring Period	Location	Response Period
Pettitt <i>et al.</i> [1999]	25/08/1999 to 18/09/1999	DA3551G01 and DA3545G01	Excavation
Haycox <i>et al.</i> [2005a]	20/03/2003 to 09/10/2003	DA3545G01	1
	29/04/2004 to 31/03/2005	DA3545G01	1, 2
Haycox <i>et al.</i> [2005b]	01/04/2005 to 30/09/2005	DA3545G01	2, 3
Haycox <i>et al.</i> [2006]	01/10/2005 to 31/03/2006	DA3545G01	3, 4

A temporary ultrasonic array was installed around the rock volume when deposition hole DA3545G01 and its neighbour DA3551G01 were first excavated in September 1999 [Pettitt *et al.*, 1999]. A total of 2467 AE triggers were obtained during monitoring of the two deposition holes. Of these 1153 were located. There was significantly more AE activity around the second deposition hole (labelled DA3545G01) than the first (DA3551G01). This difference is likely to depend upon intersection of the excavation with a greater number of pre-existing fractures. These fractures may be preferentially located in the side wall of the deposition hole or preferentially orientated to the *in situ* stress field. Fracturing associated with excavation-induced stresses was observed with AEs distributed mainly in regions orthogonal to the maximum principal stress, σ_1 . This was consistent with observations from the Canister Retrieval Tunnel and from dynamic numerical models. AEs, and hence microcrack damage, were shown to locate in clusters down the deposition hole and not as a continuous 'thin skin'. Pettitt *et al.*[2000] showed that these clusters were associated with weaknesses in the rock mass generated by

excavation through pre-existing fractures. Damage in the side wall of the deposition holes depended significantly on these pre-existing features. The *in situ* stress field was a contributing factor in that induced stresses were sufficiently high to create damage in these weakened regions although not sufficiently high to create significant damage in the rock mass as a whole.

A permanent ultrasonic array, with transducers grouted into instrumentation boreholes, was installed in the rock mass in June 2002. In this arrangement, ultrasonic monitoring has been conducted between 20th March and 9th October 2003, and then from 29th September 2004 to the present. A gap in monitoring occurred when the ultrasonic acquisition system was used for another experiment in the HRL (Pillar Stability Experiment). Processing and reporting of results has been undertaken by *Haycox et al.*[2005a], *Haycox et al.*[2005b] and *Haycox et al.*[2006] and is further discussed in Section 4.2. A description of instruments measuring other environmental factors (such as temperature and pressure) and their locations can be found in *Goudarzi and Johannesson*[2006].

Appendix II Methodology

Data Acquisition

The ultrasonic array consists of twenty-four ultrasonic transducers configured as eight transmitters and sixteen receivers installed into four instrumentation boreholes. The transducers are fixed into the boreholes using specially designed frames (Figure 4-13) – two transmitters and four receivers per frame. The boreholes are vertical, 76mm in diameter and approximately 10 meters in length distributed around each deposition hole volume. The array has been designed so as to provide good coverage for AE locations and to provide ‘skimming’ ray paths that pass within a few centimetres of the deposition-hole wall so as to sample the rock immediately adjacent to the deposition-hole wall. The layout of the instrumentation boreholes is shown in Figure 4-14 and described further in Table 4-4. Each of the ultrasonic transducers has a hemispherical brass cap fixed over its active face and is then spring-loaded against the borehole surface so as to obtain good coupling to the rock mass. The boreholes have then been filled with a slightly expansive grout so as to permanently fix the transducers in place, reduce the likelihood of damage to the transducers and to remove the borehole voids.



Figure 4-13: Top: Schematic diagram of the locations of all transducers on a single frame. Left: Photo of a section of the transducer assembly. Right: The transducer assembly during installation.

The piezoelectric transducers operate by converting a transient elastic wave into an electric signal or visa versa. The monitoring system is then operated in one of two modes. The first is used to passively monitor AE activity preferentially within the array volume. AEs release elastic energy in the same way as 'earthquakes' but over a very small scale. At these frequencies AEs have a moment magnitude (M_w) of approximately -6. They occur either during the creation process of new fractures within the medium, or on pre-existing fractures due to small scale movements. Each receiver has a frequency response of approximately 35-350kHz and contains a 40dB pre-amplifier. This minimises a reduction in signal-to-noise between the sensors and the acquisition system. The sensors have a vulcanised surround and a high pressure reinforced cable to protect them from water infiltration. In addition, polyamide tubes and *Swagelok* connectors have been fitted to the cables to reduce the likelihood of breakage.

Figure 4-15 shows a schematic diagram of the acquisition system used. Cables from each transducer pass through the pillar between the PRT and the G-tunnel. Data acquisition uses a Hyperion Ultrasonic System controlled by a PC, set up within a cabin provided by SKB. This has 16 receiving channels and 8 transmitting channels. An AE is recorded when the amplitude of the signal on a specified number of channels exceeds a trigger threshold within a time window of 5ms. The system then records the full-waveform signals from all 16 transducers. In this case a trigger threshold of 50mV on three channels was used. This allows the system to have sufficient sensitivity to record high quality data without recording an abundance of activity that cannot be processed due to very small signal to noise on only a few channels. The captured signals are digitised with a sampling interval of 1 μ s and a total length of 4096 data points. In general, low noise levels were observed (<2mV) giving high signal to noise and good quality data. AE monitoring is set to switch off during daytime working hours (6am-8pm) so as to minimise the amount of noise recorded from human activity.

A second operating mode actively acquires ultrasonic waveforms by scanning across the volume. This allows measurements of P- and S-wave velocities and signal amplitudes over a possible 128 different ray paths. By repeating these ultrasonic surveys at increments in time, a temporal analysis is obtained for the variation in medium properties. Ultrasonic surveys are conducted daily at 1am in order to measure changes in P- and S-wave signals. At that time of night, no human activity will cause noise that can interfere with the signals received. A Panametrics signal generator is used to produce a high frequency electric spike. This is sent to each of the 8 transmitters in turn. The signal emitted from each transmitter is recorded over the 16 receivers in a similar fashion to that described above. An external trigger pulse from the signal generator is used to trigger the acquisition system and identifies the transmission start time to an accuracy of one sample point. In order to decrease random noise the signal from each transmitter is stacked 100 times.

Table 4-4: Boreholes used for AE monitoring of deposition hole DA3545G01.

SKB Borehole designation	ASC Borehole reference	Transducer Numbers
KA3543G01	1	T1, T2, R1-R4
KA3545G02	2	T3, T4, R5-R8
KA3548G03	3	T5, T6, R9-R12
KA3548G02	4	T7, T8, R13-R16

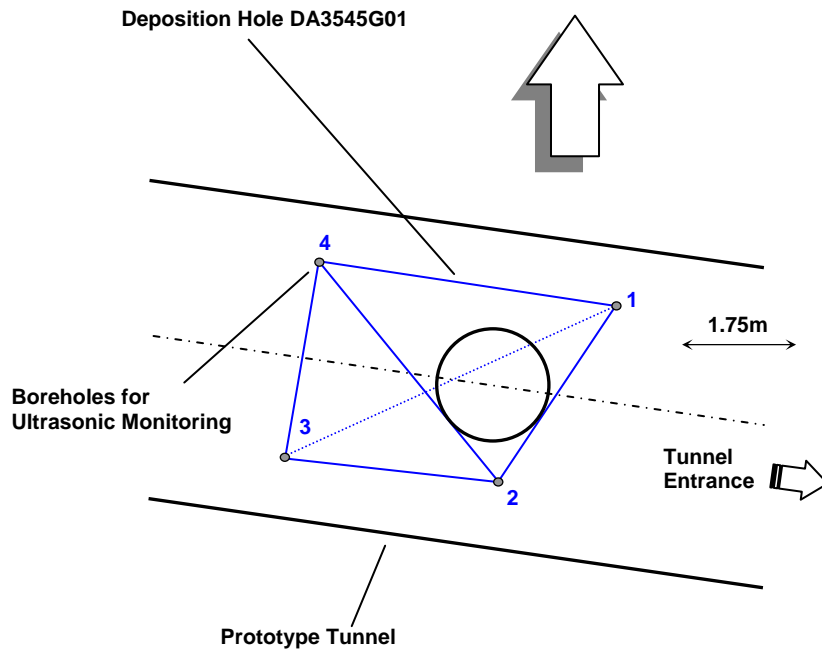


Figure 4-14: Plan view of the array geometry for Deposition Hole DA3545G01 during heating in the Prototype Tunnel. The blue solid lines represent direct raypaths between sondes illustrating their ‘skimming’ nature. The blue dashed line represents a raypath that travels through the deposition hole.

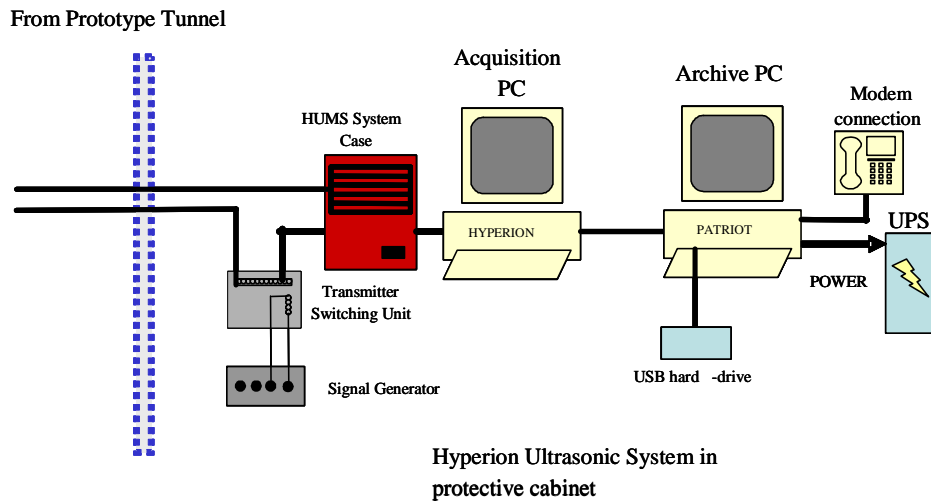


Figure 4-15: Schematic diagram of the hardware used for the heating stage in the Prototype Repository. The ultrasonic pulse generator sends a signal to each transmitter and the resulting signal is recorded on each receiver. The receivers are also used to listen for AE activity. The archive PC is required to make a copy of the data for backup purposes.

Processing Procedure

Overview

ASC's InSite Seismic Processor has been used to automatically process both the AE and ultrasonic survey data. Appendix IIIA and Appendix IIIB give the processing parameters used. *Pettitt et al.*[2005] provides a detailed description of this software.

Ultrasonic Data Procedure

The ultrasonic survey full-waveform data was initially stored with the AE data. This was automatically sorted and the survey data extracted to a separate processing project. A 'reference' survey from the previous monitoring period was used, and imported into the project. The P- and S-wave arrivals were manually picked during the previous monitoring period. Knowing the transmitter and receiver locations, the ultrasonic velocity for each ray path was calculated with an estimated uncertainty of $\pm 30 \text{m.s}^{-1}$ (± 3 data points). A cross-correlation procedure was then used to automatically process subsequent surveys. This technique cross-correlates P- and S-wave arrivals from a transmitter-receiver pair with arrivals recorded on the same transmitter-receiver pair on the reference survey. This results in high-precision measurements of P- and S-wave velocity change with estimated uncertainties of $\pm 2 \text{m.s}^{-1}$ between surveys. Note that when the transmitter and receiver are on the same borehole, the raypath is not used due to the introduction of transmission effects from the instrumentation borehole, grout and transducer frames.

The main reason for the reduction of uncertainty when using the cross-correlation procedure is the dependency of manual picking on the user's judgement of the point of arrival. This can usually be quite indiscriminate because of random noise superimposed on the first few data points of the first break. Additionally, the procedure is run automatically without any loss of precision resulting in efficient waveform processing. The cross-correlation procedure then allows for a high-resolution analysis to be performed and hence small changes in velocity to be observed. This is extremely important when changes in rock properties occur over only a small section (5%) of the ray path.

Figure 4-16 gives example waveforms recorded from one of the transmitters during this reporting period. Each waveform is first automatically picked to obtain an estimate of the P-wave or S-wave arrival. A window is then automatically defined around the arrival and a bell function is applied, centred on the automatic pick. The data at the ends of the window then have a much smaller effect on the cross-correlation. The windowed data is then cross-correlated [*Telford et al.*, 1990] with a similar window constructed around the arrival on the reference survey. The change in arrival time is then converted to a change in velocity knowing the manually-picked arrival time for the reference survey. Waveforms that do not provide automatic picks are not cross-correlated. This gives an automatic discrimination of signals that have very poor signal to noise ratios and could give spurious cross-correlation results from poor discrimination of the first arrival. During the automatic processing an arrival amplitude is also calculated from within a processing window defined by a minimum and maximum transmission velocity. This provides a robust measure of arrival amplitudes between surveys.

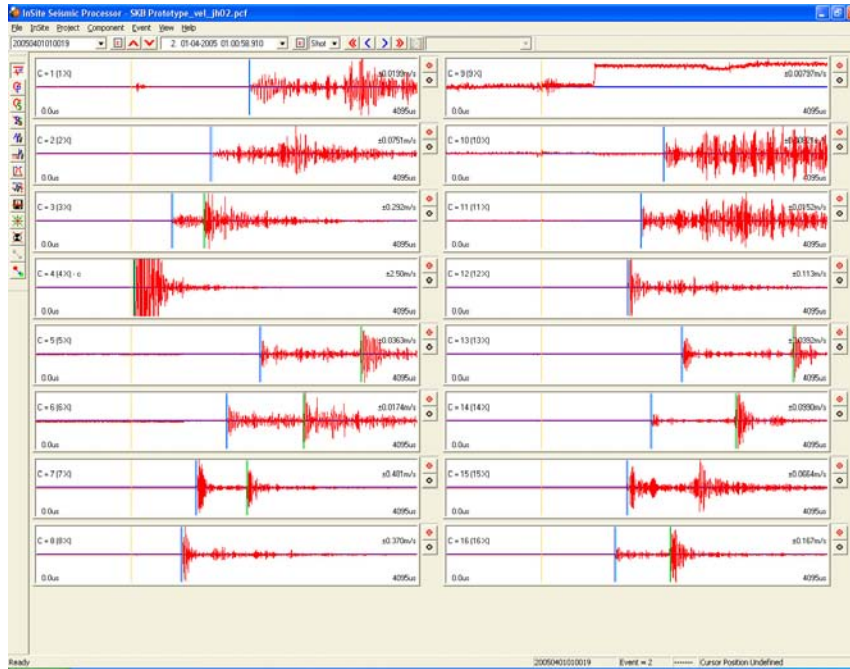


Figure 4-16: Waveforms recorded from one transmitter on the array of sixteen receivers. The gold markers indicate the transmission time. The blue and green markers indicate picked P- and S-wave arrivals respectively.

When calculating average velocities and amplitudes, raypaths passing through the deposition hole are removed due to the uncertain transmission paths produced by the wave travelling in the rock around the deposition hole and through the bentonite, fluid and canister fill. Therefore the majority of raypaths between boreholes 1 and 3 (transmitters 1, 2, 5, 6 and receivers 1, 2, 3, 4) are not used in the analysis. An exception is made for the deepest raypaths that pass under the deposition hole entirely through rock.

The dynamic Young's modulus E , and dynamic Poisson's Ratio, ν , can be calculated from the velocity measurements using Equation 1 and Equation 2

$$E = \rho V_S^2 \left(\frac{3V_P^2 - 4V_S^2}{V_P^2 - V_S^2} \right) \quad \text{Equation 1}$$

$$\nu = \frac{V_P^2 - 2V_S^2}{2(V_P^2 - V_S^2)} \quad \text{Equation 2}$$

V_P and V_S values are also used to model for crack density (c) and saturation (s) in the rock mass using the method of *Zimmerman and King*[1985]. The crack density parameter is defined by the number of cracks (penny-shaped) per unit volume multiplied by the mean value of the cube of the crack radius (Equation 3). This method assumes the elastic modulus E and ν in the damaged material normalized to the undisturbed material, decrease exponentially with crack density. Also assumed are the shear modulus (μ) is unaffected by s , and the bulk modulus (k) increases linearly with s , equalling that of uncracked rock when $s=1$. Equation 4 shows the calculation used to determine saturation.

$$c = \frac{9}{16} \ln \left(\frac{2\mu}{E_0 - 2\mu\nu_0} \right) \quad \text{Equation 3}$$

$$s = \frac{k(c,s) - k(c,0)}{k_0 - k(c,0)} \quad \text{Equation 4}$$

The calculations require an estimation of the completely undisturbed rock (i.e. an unsaturated, uncracked, intact rock mass). This study assumes values of $V_{OP} = 6660 \text{m.s}^{-1}$, and $V_{OS} = 3840 \text{m.s}^{-1}$ for the undisturbed material taken from laboratory tests on a similar granite, summarized in *Maxwell and Young*[1995]. A value of 2650 kg m^{-3} is presented by *Pettitt et al.*[2002] for the density of the rock mass.

The calculations of Young's Modulus and Poisson's ratio from measured velocities makes an assumption of an isotropic elastic medium. Under this assumption a rock can be completely characterised by two independent constants. One case of an isotropic elastic medium is a rock with a random distribution of cracks embedded in an isotropic mineral matrix. Under the application of a hydrostatic compressive stress, the rock will stay isotropic but become stiffer (which will become characterised by increased velocity V_P , V_S and therefore increased Young's modulus). In contrast, under the application of a uniaxial compressive stress, cracks with normals parallel or nearly parallel to the applied stress will preferentially close and the rock will take on a transversely isotropic symmetry. Under this situation P- and S-wave velocities become variable with orientation. The crack density and saturation calculations also assume an isotropic elastic medium.

It should be noted that E and ν calculated in this report are dynamic measurements due to the small strains exerted on the rockmass at high frequencies from the passing ultrasonic waves. Static E and ν measurements, made from uniaxial laboratory tests on rock samples, may be different from dynamic values – even if sample disturbance is minimal – due to the larger strains exerted over relatively long periods of time.

Acoustic Emission Procedure

The procedure used to process the AEs in this reporting period has been undertaken as follows:

1. Calibration surveys from the installation phase (when the deposition hole was open) have been used to optimise an automatic picking and source location algorithm and check location uncertainties. ASC's InSite seismic processing software was used for location and visualisation.
2. Where possible, P- and S-wave arrival times were measured for each AE using the automatic picking procedure.
3. AEs with ≥ 6 P-wave arrival times were input into a downhill-simplex location algorithm [*Pettitt et al.*, 2005]. This has the option of incorporating either a three-dimensional anisotropic velocity structure or an isotropic structure. Velocities calculated from the ultrasonic surveys were used.

4. The waveforms from all events were visually inspected to ensure they were 'real' acoustic emissions. Events were removed if they had the appearance of noise spikes (increase in amplitude is recorded on all channels at the same time) or they were the result of human noise (long period events that occur at close intervals during the day).
5. The acoustic emissions that remained had their arrivals manually picked to obtain the best possible location. Any events that located outside the expected region of activity were further checked to ensure accuracy. Experience from previous studies around deposition holes showed that large source location errors were produced if significant portions of a ray path passed through the excavated deposition hole void. This only becomes a problem for the largest AEs. AEs were reprocessed with these ray paths removed.
6. Finally, a filter was applied to remove all AEs with a location error greater than 1.0.

During the equipment installation phase, calibration shots have been undertaken to assess the sensitivity of the system to 'real' AEs and to determine the accuracy with which real events could be subsequently located by the array of sensors. A series of test 'shots' were performed on the wall of deposition hole DA3545G01 (Figure 4-17). The shots consisted of undertaking 10 'pencil lead breaks' and 10 hits with a screw-driver at 1 metre intervals down 4 lines along the deposition hole wall. The pencil-lead tests involved breaking the 0.5 mm lead from a mechanical pencil against the borehole wall. This is a 'standard' analogue for an AE as it generates a similar amount of high-frequency energy. An example of a pencil lead break test is shown in Figure 4-18. This was made at 6 metres below the tunnel surface on the deposition hole wall at a point adjacent to borehole KA3548G02. This corresponds to an AE source dimension on the millimetre scale (grain size).

The screw-driver hits provided a good amplitude signal for assessing the accuracy with which events can be located within the volume surrounded by the array. Figure 4-17 shows the results from one processed set of locations for a line of shots down the deposition hole wall. This shows that the array is able to locate events with good accuracy and consistency within an estimated uncertainty of approximately 10cm.

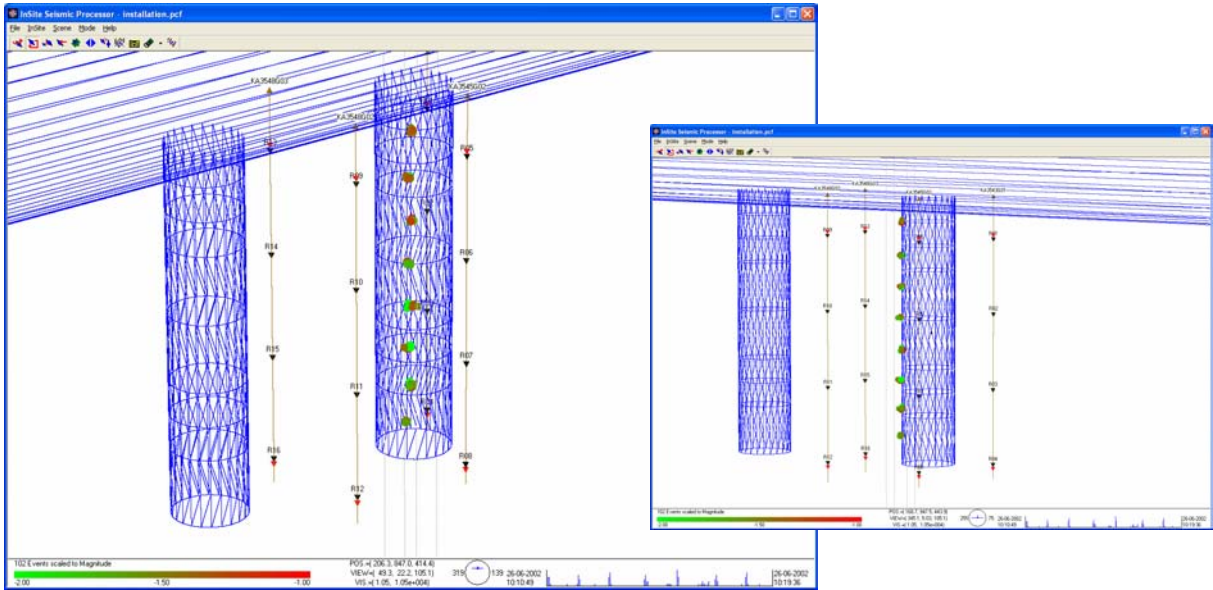


Figure 4-17: Locations of calibration shots obtained from a series of tests at 1 metre intervals down the wall of deposition hole DA3545G01. The two views show that these line up and are located close to the surface of the hole.

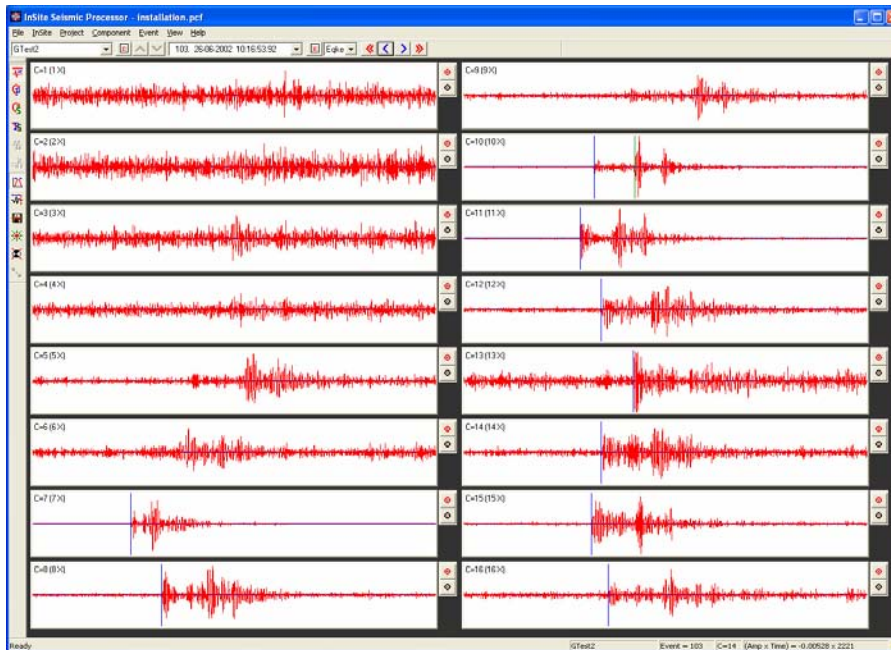


Figure 4-18: Example waveforms from each of the 16 receiving channels for a ‘pencil-lead break’ test undertaken against the Deposition Hole (DA3545G01) wall 6 metres below the tunnel floor.

Appendix III Processing Parameters

B: Ultrasonic survey processing parameters:

PROCESSING PARAMETERS

Velocity survey processing

EVENT INITIALISATION	
View/process waveforms by	Channel
Channel-view Width-to-height ratio	6
Waveform Response type	Set from sensor
Sampling time	1
Time units	Microseconds
Pre-signal points	200
Spline sampling time	0.2
Waveform To point	1023
P-Time correction	0
S-Time correction	0
Automatically update Channel Settings	NOT SET
Project Files	NULL

AUTO PICKING	
Allow P-wave-autopicking	YES, Use first peak in the auto-pick function
Back-window length	100
Front-window length	35
Picking Threshold	4
Min. Peak-to-Peak amplitude	0
Allow S-Wave Autopicking	YES, Use first peak in the auto-pick function
Back-window length	100
Front-window length	35
Picking Threshold	5
Min. Peak-to-Peak amplitude	0
Allow Automatic Amplitude Picking	YES
Use Velocity Window Picking	YES
P-wave Min. Velocity/Max. Velocity	4500, 6500
S-wave Min. Velocity/Max. Velocity	2500, 3500

CROSS-CORRELATION	
CCR Events	Referenced to a Survey
Reference Component	20041208005920
Reference Event	NULL
Window construction method	Front to Back
Window comparison method	Fixed to reference picks
Window Parameters	Back-window length = 20 Front-window length=30 Rise-time multiplier = NULL Power to raise waveform =1 Split to a Spline function = YES Obtain absolute waveform= NOT SET

LOCATER	<i>(not used in velocity surveys)</i>
Method	SIMPLEX INTO GEIGER
Method settings Simplex settings Geiger settings	Tolerance = 0.01 LPNorm = 1 P-wave weighting = 1 S-wave weighting = 1 Use Outlier Identification = NOT SET Arrival error factor = x2 Tolerance (Loc. units) = 0.01 Step size (Loc.units) = 0.1 Max. Iterations = 100 Conditional No. Limit = 1000000000
Velocity Structure	Homogeneous Isotropic
Velocity Structure settings	P-wave velocity = 5973.85 m.s ⁻¹ S-wave velocity = 3342.705 m.s ⁻¹ Attenuation = 200 Q(S) value = 100
Data to use	P-wave Arrivals Only
Distance units	Metres
Working time units	Microseconds
Min P-wave arrivals	0
Min S-wave arrivals	0
Min Independent arrivals	5
Max. Residual	20
Start point	Start at the centroid of the array
Write report to RPT	NOT SET
Source parameters	Set to calculate automatically

A: AE processing parameters:

PROCESSING PARAMETERS

AE processing

EVENT INITIALISATION	
View/process waveforms by	Channel
Channel-view Width-to-height ratio	6
Waveform Response type	Set from sensor
Sampling time	1
Time units	Microseconds
Pre-signal points	200
Spline sampling time	0.2
Waveform To point	1023
P-Time correction	0
S-Time correction	0
Automatically update Channel Settings	SET
Project Files	NULL

AUTO PICKING	
Allow P-wave-autopicking	YES, Use max peak in the auto-pick function
Back-window length	100
Front-window length	35
Picking Threshold	5
Min. Peak-to-Peak amplitude	0
Allow S-Wave Autopicking	YES, Use max peak in the auto-pick function
Back-window length	100
Front-window length	35
Picking Threshold	5
Min. Peak-to-Peak amplitude	0
Allow Automatic Amplitude Picking	NOT SET
Use Velocity Window Picking	YES
P-wave Min. Velocity/Max. Velocity	4500, 6500
S-wave Min. Velocity/Max. Velocity	2500, 3500

CROSS-CORRELATION	<i>(not used in AE processing)</i>
CCR Events	NOT SET
Reference Component	NOT SET
Reference Event	NULL (not activated)
Window construction method	Individual
Window comparison method	Fixed to reference picks
Window Parameters	Back-window length = 31 Front-window length = 31 Rise-time multiplier = NULL Power to raise waveform =1 Split to a Spline function = NOT SET Obtain absolute waveform= NOT SET

LOCATER	
Method	SIMPLEX INTO GEIGER
Method settings Simplex settings Geiger settings	Tolerance = 0.01 LPNorm = 1 P-wave weighting = 1 S-wave weighting = 1 Use Outlier Identification = NOT SET Arrival error factor = x2 Tolerance (Loc. units) = 0.01 Step size (Loc.units) = 0.1 Max. Iterations = 100 Conditional No. Limit = 1000000000
Velocity Structure	Homogeneous Isotropic
Velocity Structure settings	P-wave velocity = 5985 m.s ⁻¹ S-wave velocity = 3343 m.s ⁻¹ Attenuation = 200 Q(S) value = 100
Data to use	P-wave Arrivals Only
Distance units	Metres
Working time units	Microseconds
Min P-wave arrivals	0
Min S-wave arrivals	0
Min Independent arrivals	5
Max. Residual	20
Start point	Start at the centroid of the array
Write report to RPT	NOT SET
Source parameters	Set to calculate automatically

EVENT FILTER	
Date and Time	NOT SET
Location volume	Minimum = (235, 880, 420)
	Maximum = (300, 964, 463)
L. Magnitude	NOT SET
Location Error	1
Independent Instruments	Minimum = 0

SOURCE PARAMETERS	
Automatic source-parameter windows	P-wave back window = 10
	P-wave front window = 50
	S-wave back window = 10
	S-wave front window = 50
Source parameter calculations	Min number to use = 3
Automatic source-parameter windows	Apply Q correction = SET
	Source density = 2640
	Source shear modulus = 39131400000
	Av. radiation coefficient: $F_p = 0.52$, $F_s = 0.63$
Source parameter calculations	Source coefficient: $k_p = 2.01$, $k_s = 1.32$
Magnitude calculations	Instrument magnitude = $1 * \log(\text{ppV}) + 0$
	Moment magnitude = $0.666667 * \log(M_0) + -6$

